PHYSIOLOGY

Impact of aging and oxidative stress on specific components of excitation contraction coupling in regulating force generation

Hongyang Xu[1], Bumsoo Ahn[1,2], Holly Van Remmen[1,3]*

Muscle weakness associated with sarcopenia is a major contributor to reduced health span and quality of life in the elderly. However, the underlying mechanisms of muscle weakness in aging are not fully defined. We investigated the effect of oxidative stress and aging on specific molecular mechanisms involved in muscle force production in mice and skinned permeabilized single fibers in mice lacking the antioxidant enzyme CuZnSod (*Sod1*KO) and in aging (24-month-old) wild-type mice. Loss of muscle strength occurs in both models, potentially because of reduced membrane excitability with altered NKA signaling and RyR stability, decreased fiber Ca^{2+} sensitivity and suppressed SERCA activity via modification of the Cys^{674} residue, dysregulated SR and cytosolic Ca^{2+} homeostasis, and impaired mitochondrial Ca^{2+} buffering and respiration. Our results provide a better understanding of the specific impacts of aging and oxidative stress on mechanisms related to muscle weakness that may point to future interventions for countering muscle weakness.

INTRODUCTION

Aging-induced sarcopenia is a major cause of morbidity and mortality in the elderly population and is characterized as loss of muscle mass and strength (*1*). However, loss of muscle strength is not solely attributed to muscle atrophy, as it has been reported that muscle weakness occurs earlier and progresses faster than the atrophy (*2*). Furthermore, mice with altered expression of superoxide dismutase (*Sod1* or *Sod2*) are effective tools to study the effects of oxidative stress on skeletal muscle function and metabolism. In previous studies, we have used whole-body and tissue-specific conditional knockout models for both the cytosolic *CuZnSod* (*Sod1*) and mitochondrial superoxide dismutase *MnSod* (*Sod2*) targeted to neurons and in skeletal muscle (*3*–*11*). In the current study, we are using the *Sod1*KO mouse (mice lacking *CuZnSod* in all tissues) that we have characterized extensively, reporting muscle atrophy and weakness that resemble the aging muscle phenotypes present in old wild-type (WT) mice (*9*–*11*). Our previous studies using muscle-specific deletion of either *Sod1* or *Sod2* have shown that muscle weakness can occur even without atrophy (*3*, *4*). These findings suggest that the decline in force production during sarcopenia is due to intrinsic deficits of force-generating properties of muscle rather than an indirect consequence of muscle atrophy. Recently, using *Sod1*KO mice (*1*) or in denervation-induced sarcopenia (*12*, *13*), our group has reported a direct correlation between elevated cellular oxidative stress and muscle weakness and oxidative damage to components of the excitation-contraction coupling (E-C coupling) system, the major mechanism for force generation in muscle. These findings suggest that increased cellular oxidative stress is a key factor in muscle weakness. However, the specific mechanisms involved, particularly those that impair E-C coupling components, remain unclear.

Skeletal muscle produces force through E-C coupling, where a sequence of events is involved, initiating from the electrical conduction of an action potential on the sarcolemmal membrane to the sensing of this action potential in transverse tubules (t-tubules) to trigger the release of Ca^{2+} ions from sarcoplasmic reticulum (SR) and eventually to the binding of Ca^{2+} ions to the contractile filaments to induce the final force production (*14*). Within the E-C coupling system, there are many molecules and structures involved, such as sarcolemma and t-tubules for maintaining the membrane potential and conducting the action potential, the SR proteins ryanodine receptor (RyR; calcium release channel), calsequestrin (CSQ; for Ca^{2+} storage in SR), and SR Ca^{2+}–adenosine triphosphatase (ATPase) (SERCA; for pumping the Ca^{2+} back into SR) for governing cellular calcium homeostasis through release and reuptake of Ca^{2+} ions in and out of SR, and the contractile proteins (myosin, actin, troponin, etc.) for finally producing force. To further and more directly probe the role of these components individually in muscle weakness, we used a mechanically skinned single muscle fiber preparation that allows us to detect changes in specific molecular or structural components involved in the E-C coupling process in sarcopenic mouse models with high oxidative stress, i.e., *Sod1*KO mice and aging mice.

The goal of this study was to investigate the effect of aging and oxidative stress on specific components and mechanisms contributing to muscle weakness in sarcopenia at the whole muscle and single fiber levels. In this study, we used both *Sod1*KO (the whole-body knockout model; 12-month-old) and old WT (24-month-old) mice to study aging- and oxidative stress–induced sarcopenia phenotypes. We identified impaired contractile function, membrane excitability, and dysregulated cellular calcium homeostasis associated with oxidative damage to the SERCA protein; decreased calcium sensitivity of contractile filaments; reduced SR calcium storage; and damaged mitochondrial function and calcium metabolism. Muscle from both *Sod1*KO and aging mice showed a substantial loss of force when measured at the whole muscle level, yet contractile function measured at the skinned fiber level in response to maximum Ca^{2+} activation showed no deficit in aging mice, suggesting that additional factors extrinsic to contractile filaments contribute to weakness in older muscle. In muscle from *Sod1*KO mice, weakness

[1]Aging and Metabolism Research Program, Oklahoma Medical Research Foundation, Oklahoma City, OK, USA. [2]Department of Internal Medicine, Wake Forest School of Medicine, Winston-Salem, NC, USA. [3]Oklahoma City VA Medical Center, Oklahoma City, OK, USA.
*Corresponding author. Email: holly-vanremmen@omrf.org

is apparent at both whole muscle and skinned fiber levels when activated with maximum Ca^{2+}, suggesting a direct impact of elevated oxidative stress at the contractile filaments, along with other E-C coupling components in the single fiber level that translates to whole muscle weakness.

Our findings confirmed the importance of oxidative stress in E-C coupling impairment in muscle strength and support a critical role for factors extrinsic to only contractile filaments in muscle weakness in aging. This study may inform future development of interventions to interact with these molecular targets to improve muscle strength in elderly people.

RESULTS

Neuromuscular junction function and muscle force generation at the whole muscle level are impaired in *Sod1*KO and aging mice

Muscle force production and neuromuscular junction (NMJ) function were measured using in situ electrical stimulation in gastrocnemius (GTN) muscle as we have previously described (*15*). In *Sod1*KO and older female WT mice, both muscle weight and absolute maximum force production (194 mg and 1.02 N for *Sod1*KO mice and 252 mg and 1.55 N for old WT mice) were found decreased markedly compared to adult female 12-month-old WT mice (296 mg and 2.25 N; Fig. 1, A and B). After the force measurements were completed, the specific maximum force was calculated by the length and weight of the GTN muscle as described in Materials and Methods. In *Sod1*KO and aging mice, we found that the maximum specific force (16 N/cm^2 for adult *Sod1*KO mice and 19 N/cm^2 for old WT mice) decreased markedly compared to younger WT mice (25 N/cm^2; Fig. 1C). The specific impact on NMJ function was determined by normalizing the force generated using nerve stimulation through the NMJ to force generated by direct muscle stimulation, bypassing the NMJ. In agreement with previous studies from our laboratory and other colleague laboratories (*15*–*18*), NMJ function in the *Sod1*KO and older mice is significantly impaired, resulting in a ~30 and 15% functional denervation, respectively (i.e., nerve force/muscle force = 70%; Fig. 1D). In contrast, 12-month-old adult WT mice show a nerve/muscle directed force ratio close to 100%, indicative of full NMJ function (Fig. 1D). Confocal microscopy images support these findings, showing that the structure of the NMJ in *Sod1*KO mice is severely damaged with fragmentation and denervation, while in aging mice, the NMJ impairment is better than in *Sod1*KO mice but morphologically still worse than in adult WT mice (Fig. 1, E to H). Specifically, the quantification and statistical analysis indicate that the NMJ area is smaller in *Sod1*KO (722 μm^2) and aging mice (742 μm^2) compared to adult WT mice (849 μm^2), the proportion of fragmented NMJ is remarkably higher in *Sod1*KO mice (74%) and aging mice (29%) than in WT mice (11%), and the percentage of denervated NMJs is markedly higher in both *Sod1*KO mice (96%) and aging mice (33%) compared to WT mice (0.7%) (Fig. 1, F to G).

Force production and cross-bridge ATPase activity measured at the single fiber level are reduced in *Sod1*KO mice but not compromised in fibers from aging WT mice

Single fiber–specific force production was assessed in individual skinned fast-twitch muscle fibers from WT, *Sod1*KO, and aging mice, and the specific force in a skinned fiber was defined as the force produced (in mN) in maximum Ca^{2+} activation solution [i.e., at 20 μM free Ca^{2+} (pCa 4.7)], normalized to the fiber cross-sectional area (in mm^2), and then expressed in units of mN/mm^2. This preparation bypasses all E-C coupling and NMJ components and measures the impact of the contractile filaments alone. In muscle fibers from *Sod1*KO mice, the specific force (153 mN/mm^2) is much lower than in muscle fibers from adult WT mice (268 mN/mm^2) (Fig. 2A), which is similar to our results measured at the whole muscle level in situ. In muscle fibers from aging mice, the specific force (266 mN/mm^2) is the same as in the younger WT muscle fibers (Fig. 2A), in contrast to the decreased specific force when measured at whole muscle level. The ATPase activity of cross-bridges was detected by measuring the production rate of the inorganic phosphate (P_i) at both resting and Ca^{2+}-activated (3 mM Ca^{2+}) status in myosin heavy chain (MHC) extract from GTN muscle. The cross-bridge ATPase activity is markedly decreased in muscle from *Sod1*KO mice (0.13 resting/0.17 Ca^{2+} activated) compared to muscle from adult WT mice (0.17 resting/0.26 Ca^{2+} activated) and muscle from aging WT mice (0.16 resting/0.25 Ca^{2+} activated), and there is no significant difference between adult and aging WT muscles (Fig. 2B).

Calcium sensitivity of contractile filaments in fast-twitch muscle fibers is significantly lower in *Sod1*KO and aging mice and also with less reaction to *S*-glutathionylation

The calcium sensitivity of contractile filaments was assessed in single skinned fast-twitch muscle fibers by activating the contractile apparatus in a series of solutions with free [Ca^{2+}] heavily buffered at successively higher levels (pCa > 10 to 4.7, denoted by arrows in Fig. 3A) to elicit progressively greater force production (Fig. 3A). On the basis of this, a force-pCa curve can be plotted, showing a progressively greater force under the increasing Ca^{2+} concentration (Fig. 3B). Using the force-pCa curve, the pCa50, or the value of calcium concentration at which the fiber produces half of the maximum force, can be obtained. The pCa50 is commonly used to describe the calcium sensitivity of the muscle contractile apparatus. Our quantified data show that in both *Sod1*KO and aging fibers, the pCa50 value (5.82 in *Sod1*KO fibers, 5.83 in aging fibers) is significantly lower than in adult WT fibers (5.87), indicating a lower calcium sensitivity in these two groups (Fig. 3C). It has previously been shown that treatment with the sulfhydryl-specific oxidant 2,2′-dithiodipyridine (DTDP; 100 μM, 5 min), in combination with reduced glutathione (GSH; 5 mM, 2 min; referred to as DTDP-GSH treatment) in skinned fast-twitch fibers, results in *S*-glutathionylation of the troponin I (TnI) fast isoform (on the Cys^{134} residue). This modification is able to induce a significant increase in myofibrillar Ca^{2+} sensitivity, which is reversible by the treatment with dithiothreitol (DTT; 10 mM for 5 min) (*19*, *20*). To determine whether modification of TnI in fast-twitch fibers is altered by aging and oxidative stress in the *Sod1*KO and aging WT fibers, DTDP-GSH treatment was applied to skinned fast-twitch fibers in all three groups. We found a large increase in Ca^{2+} sensitivity and elevation of the pCa50 value (mean ± SD) to 0.144 ± 0.022 pCa units in young WT fibers (Fig. 3D). In contrast, although the Ca^{2+} sensitivity in *Sod1*KO and aging fibers was also increased by the DTDP-GSH treatment, the increased pCa50 value is not as high as in adult WT fibers, increasing only 0.098 ± 0.032 and 0.102 ± 0.035 pCa units, respectively (Fig. 3D), suggesting inefficient modification of the Cys^{134} residue of TnI. Last, to estimate the level of *S*-glutathionylation in fibers from the different groups, we treated the skinned fiber bundles with DTDP-GSH and detected the level of GSH associated with TnI

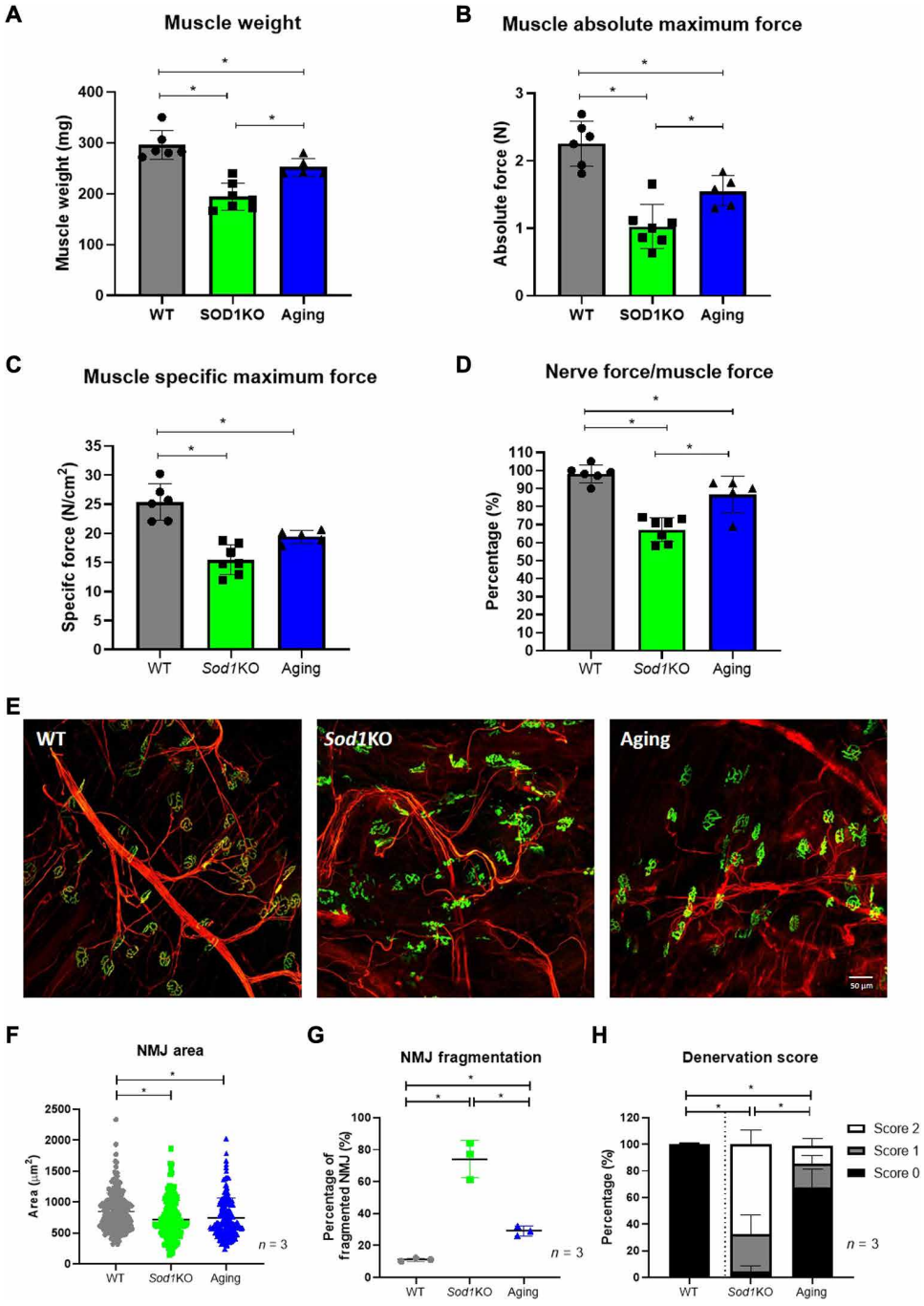

Fig. 1. Muscle and NMJ function at the whole muscle level and NMJ morphology. Muscle and NMJ function were measured with in situ electrical stimulation with GTN muscle. Muscle weight (**A**) and absolute maximum force (**B**). Muscle-specific maximum force (**C**) and normalized proportion of the maximum nerve-derived force to the maximum muscle-derived force (**D**). (**E**) Representative confocal images showing NMJ morphology in different groups as labeled. (**F** to **H**) Pooled data for the analysis of NMJ morphological parameters, including NMJ area, NMJ fragmentation, and NMJ denervation. *Significant difference between labeled groups [$P < 0.05$, one-way analysis of variance (ANOVA)]. $n = 3$ to 7 animals. Data are presented as means ± SD.

through Western blotting with nonreducing buffer (Fig. 3E). After normalizing the GSH content to the total TnI amount in that fiber bundle, we found a decreased *S*-glutathionylation of TnI in fibers from *Sod1*KO mice and aging mice compared to fibers from adult WT mice. The aging fibers showed less *S*-glutathionylation than *Sod1*KO fibers (Fig. 3F).

Membrane excitability is significantly impaired in fast-twitch fibers from *Sod1*KO and aging WT mice associated with reduced expression of critical Na^+-K^+-ATPase proteins

The measurement of membrane excitability was assessed in individual skinned fast-twitch muscle fibers from all three groups. In each skinned fiber, the membrane excitability was determined by

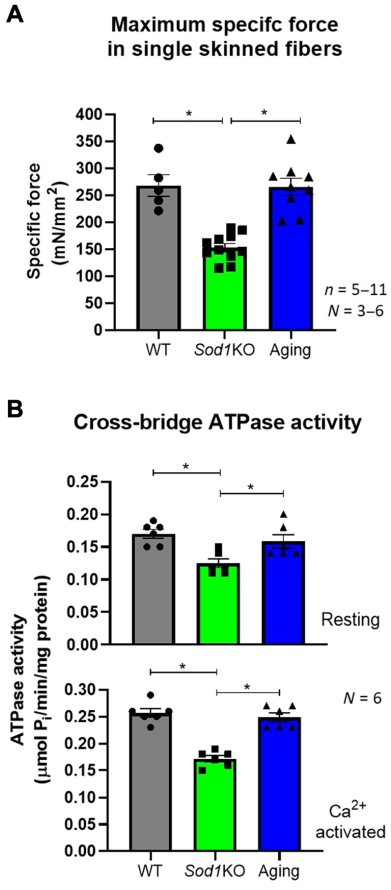

Fig. 2. Muscle maximum specific force production at the single fiber level and the cross-bridge ATPase activity. Muscle maximum specific force production was measured at the single skinned fiber level, and fiber contraction was activated by Ca^{2+} at pCa 4.6. Specific force (in mN/mm^2) was defined as maximum Ca^{2+}-activated force (in mN) normalized to fiber cross-sectional area (in mm^2). Cross-bridge ATPase activity was detected at both resting and Ca^{2+}-activated (3 mM Ca^{2+}) conditions through measuring the production rate of the P_i. (**A**) Specific muscle maximum force in different groups. (**B**) ATPase activity of cross-bridge across different groups. *Significant difference between labeled groups ($P < 0.05$, one-way ANOVA). *n* indicates the number of fibers, and *N* indicates the number of animals. Data are presented as means ± SD.

recording the force response produced by the transverse system (t-system) depolarization through ionic substitution [upon exchange of K^+-HDTA (hexa-methylene-diamine-tetraacetate) with Na^+-HDTA] and expressing the force response produced by depolarization as a percentage of the maximum Ca^{2+}-activated force production measured in that fiber. Under normal conditions, *t*-system depolarization in fast-twitch fibers is able to trigger a force response as high as close to 80% of the maximum Ca^{2+}-activated force production in that fiber (*21*, *22*), which is what we found in the adult WT fibers (Fig. 4, A and B). In contrast, the depolarization-induced force response is significantly lower in the *Sod1*KO fibers compared to adult WT fibers, triggering only 10% of the maximum force (Fig. 4, A and B). In the aging WT fibers, the depolarization-induced force response is lower than in adult WT fibers but better preserved than that in the *Sod1*KO fibers, reaching 58% of the maximum force (Fig. 4, A and B).

To investigate possible mechanisms responsible for this difference, we measured the amount of proteins potentially involved in regulating membrane excitability in whole GTN muscle homogenates including calcium release channel RyR and its stabilizer calstabin, voltage sensor dihydropyridine receptors α subunit (DHPRα), and the membrane potential keeper Na^+-K^+-ATPases (NKA) through Western blotting. RyR and DHPRα protein levels are not changed across the three groups (Fig. 4, C and E); however, the amount of calstabin, a stabilizer of RyR, is significantly lower in *Sod1*KO and aging muscles compared to adult WT muscles (Fig. 4D). NKA is present in the sarcolemma and the t-tubule membrane to maintain the ionic gradients of sodium and potassium across sarcolemma. As the predominant catalytic subunit, NKAα subunit has two major isoforms, with NKAα1 being the ubiquitous isoform appearing in all tissues and NKAα2 being the skeletal muscle–specific isoform localizing only in skeletal muscles. Changes in the amount of NKAα indicate different levels of membrane potential or a different ability for maintaining or restoring membrane potential. We measured a significant reduction (70% reduced) of NKAα1 amount in *Sod1*KO muscles compared to WT and aging muscles, and the amount of the skeletal muscle–specific isoform NKAα2 was decreased by 60% in *Sod1*KO and 40% in aging muscles, respectively, when compared to adult WT muscles (Fig. 4, F and G).

Relative SERCA activity is decreased in single skinned fast-twitch muscle fibers from *Sod1*KO and aging WT mice and less sensitive to peroxynitrite-induced *S*-glutathionylation

SERCA activity was measured in single skinned fast-twitch muscle fibers through the repletion and depletion of the SR Ca^{2+} storage. When SR Ca^{2+} storage is depleted (in 30 mM caffeine-low Mg^{2+} solution, with the presence of 0.5 mM EGTA, referred to as "release solution"), the released Ca^{2+} ions from SR will trigger a force response of that fiber and will then be bound and removed by EGTA to prevent reuptake to the SR by SERCA. Using different periods of time (15, 30, 60, 120, and 180 s) for reloading the SR Ca^{2+} storage in potassium-based HDTA (K-HDTA) solution with 1 mM total EGTA at pCa 6.7 (referred to as "loading solution"), different amounts of Ca^{2+} ions will be loaded into SR by SERCA, which will trigger different force responses upon the SR depletion. Normalizing the area under the force trace at each time point to the maximum loading time (180 s) as a percentage, we are able to plot a force–loading time curve that indicates the relative SERCA activity (Fig. 5, A to C). In agreement with our previous findings of SERCA activity in muscle homogenates, in this study, we also observed a marked decrease of the SERCA activity in *Sod1*KO and aging muscle fibers with a significant longer time (51 s in *Sod1*KO and 47 s in aging) to reach half of their maximum SR Ca^{2+} storage compared to WT fibers (40 s; Fig. 5, A to D).

In addition, previous studies have shown that SERCA activity can be regulated through peroxynitrite-induced *S*-glutathionylation (100 μM peroxynitrite for 5 min and 100 mM GSH for 2 min in K-HDTA solution) on its Cys^{674} residues, which results in a large increase in SERCA activity (*23*–*26*). Consistent with this, we found that SERCA activity was significantly elevated in adult WT fibers in response to peroxynitrite-induced *S*-glutathionylation, reaching half of the maximum SR Ca^{2+} storage in only 16 s (an increase of 60%). Similarly, in aging WT fibers, SERCA activity increased 46% (25 s to reach half maximum SR Ca^{2+} storage), although this number is still lower than in adult WT fibers. In stark contrast, in *Sod1*KO fibers, the SERCA activity had a very low response to *S*-glutathionylation

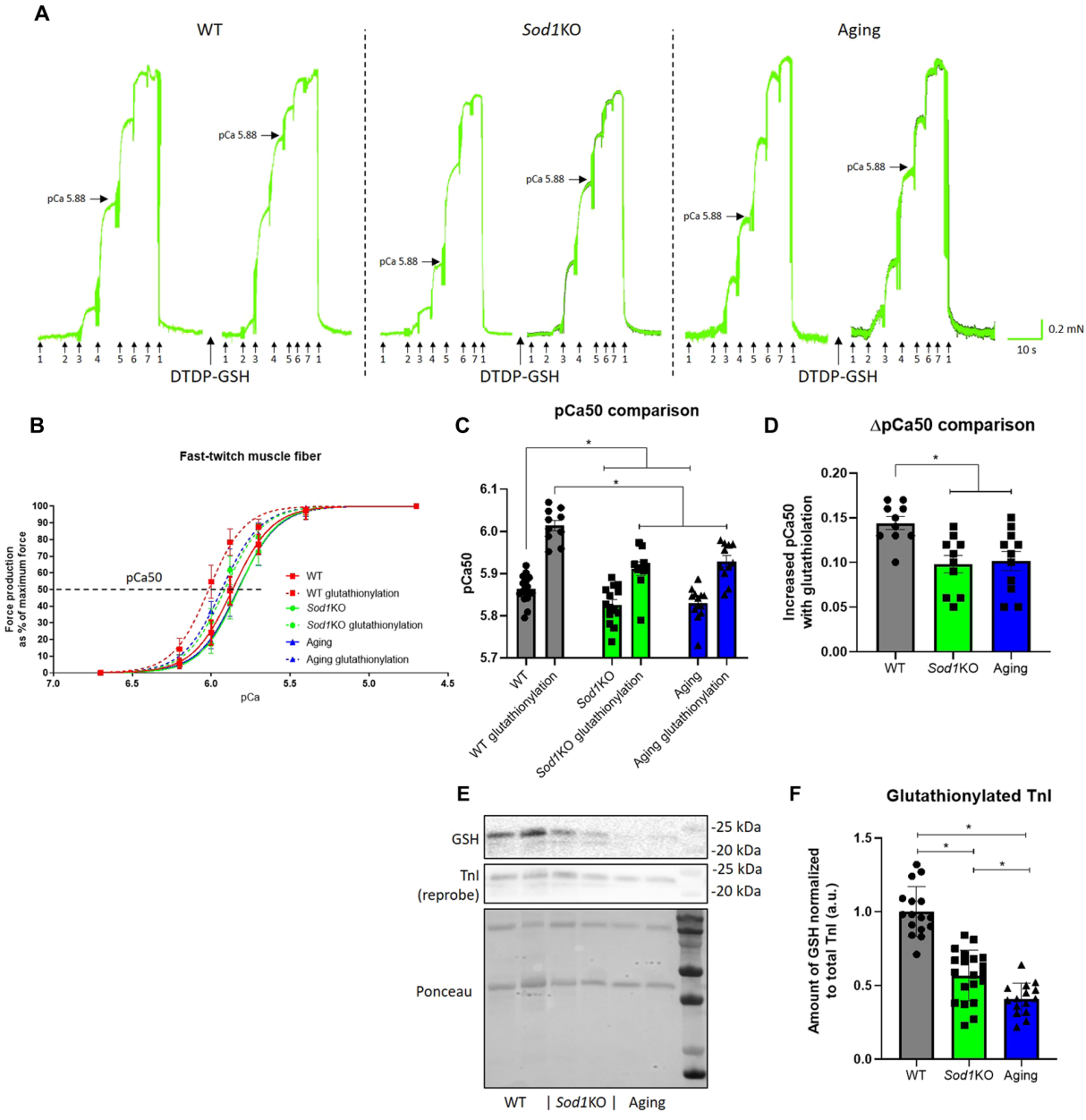

Fig. 3. Calcium sensitivity of fast-twitch muscle fibers from different groups, with and without glutathionylation. Individual skinned muscle fibers from fast-twitch muscles of different groups were activated in a series solution with progressively higher free [Ca^{2+}] from pCa > 10 to 4.7 [denoted by arrows: 1 (pCa > 10, no force), 2 (pCa 6.2), 3 (pCa 6.0), 4 (pCa 5.88), 5 (pCa 5.7), 6 (pCa 5.4), and 7 (pCa 4.7, maximum Ca^{2+}-activating solution)]. Horizontal arrows mark the force level achieved at pCa 5.88. DTDP-GSH treatments were applied at pCa > 10 with 100 μM DTDP for 5 min followed by 5 mM GSH for 2 min. (**A**) Representative force traces of single skinned fast-twitch fibers from WT, *Sod1*KO, and aging mice, before and after DTDP-GSH treatment (glutathionylation). (**B**) Force-pCa curves of different groups with and without glutathionylation. (**C**) pCa50 values (i.e., pCa giving at half maximum force) for individual fast-twitch muscle fibers in different groups with and without glutathionylation. (**D**) Changes in Ca^{2+} sensitivity (ΔpCa50) with glutathionylation treatments in fast-twitch fibers from different groups. (**E** and **F**) Representative Western blot images with pooled data for the relative amount of glutationylated TnI after DTDP-GSH treatment in skinned fiber bundles from different groups. *Significant difference between labeled groups ($P < 0.05$, one-way ANOVA). $n = 10$ to 18 indicates the number of fibers analyzed, and $N = 5$ to 9 indicates the number of animals from which the fibers were obtained. Data are presented as means ± SD. a.u., arbitrary units.

and increased only 16% (from 51 to 43 s for the time to reach half maximum SR Ca^{2+} storage; Fig. 5, A to D), indicating a lower regulating ability of their Cys^{674} residue through *S*-glutathionylation and suggesting a potential role for oxidative damage at this residue. Treatment with the compound CDN1163, a proven SERCA activator that works via an allosteric mechanism, increased SERCA activity in *Sod1*KO fibers, resulting in a greatly reduced time (30 s in *Sod1*KO, 42% increased) to reach half maximum SR Ca^{2+} storage (Fig. 5D). Last, the amount of both SERCA1 and SERCA2a proteins was performed by Western blotting in whole GTN muscle

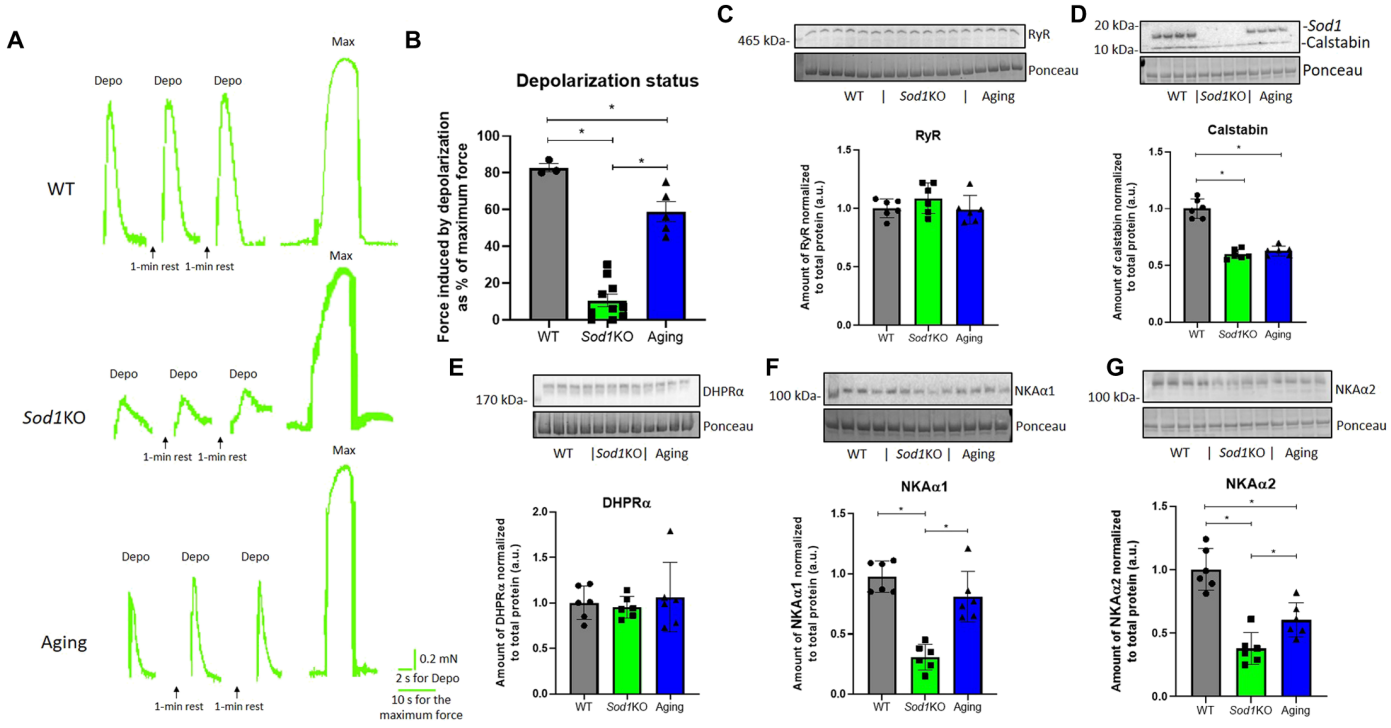

Fig. 4. Membrane excitability of fast-twitch fibers from different groups and the amount of potential relative proteins involved. Membrane excitability of a skinned fiber was assessed from the force response to depolarization induced by ionic substitution (refer as "Depo" in the figure), expressed relative to maximum Ca^{2+}-activated force (refer as "Max" in the figure) in that fiber. (**A**) Representative force trace of depolarization-induced force responses in single skinned fast-twitch fibers (upon exchange of K-HDTA with Na-HDTA solution), along with the maximum force production in that given fiber from WT, *Sod1*KO, and aging groups. (**B**) Pooled data of the depolarization-induced force responses relative to the maximum force production as a proportion. (**C** to **G**) Representative Western blot images with pooled data for the relative proteins that potentially are involved in membrane excitability, including the following from (C) to (G): RyR, calstabin, DHPRα, NKAα1, and NKAα2. *Significant difference between labeled groups ($P < 0.05$, one-way ANOVA). For the depolarization-induced force data, $n = 3$ to 10 indicates the number of fibers analyzed, and $N = 3$ indicates the number of animals from which the fibers were obtained; for the relative protein amount in Western blotting, $n = 6$ indicates the number of animals. Data are presented as means ± SD.

homogenates, and no change was observed across all three groups (Fig. 5, E and F).

Endogenous and the maximum Ca^{2+} storage in SR are lower in *Sod1*KO and aging muscles, along with altered levels of calcium storing and transporting proteins, CSQ, and parvalbumin

SR Ca^{2+} storage was measured in fiber bundles by fluorescent staining of Ca^{2+} ions using cell-permeable Fluro-5F fluorescent dye at both endogenous and maximum levels (with 180-s loading in loading solution). Ca^{2+} storage levels of SR and the fluorescent images were taken by a confocal microscope with *Z*-stacks to include all three-dimensional (3D) structure of intact fibers from that bundle. The endogenous SR Ca^{2+} storage is significantly lower in both *Sod1*KO and aging fibers compared to adult WT fibers, and in response to Ca^{2+} loading, the maximum Ca^{2+} storage of SR is also much lower in the fibers from these two groups than in adult WT fibers (Fig. 6, A and B). Western blotting shows the relative amount of SR Ca^{2+}–storing protein CSQ and cytosolic Ca^{2+}–transporting protein parvalbumin in whole GTN muscle homogenates. The CSQ amount is significantly higher in aging muscle when compared to adult WT and *Sod1*KO muscles (Fig. 6C), in agreement with our previously published results (*1*). Parvalbumin is a cytosolic Ca^{2+}–transporting protein that binds Ca^{2+} ions and transfers them to SERCA for Ca^{2+} reuptake back into SR. The amount of parvalbumin is increased markedly in both *Sod1*KO and aging muscles (Fig. 6D).

Mitochondrial calcium retention capacity and respiration are markedly impaired in *Sod1*KO and aging muscles

Mitochondrial calcium retention capacity (CRC) was assessed by challenging isolated mitochondria from GTN muscle with a sequential addition of calcium ions (2.5 μM every 1 min), in the presence of a membrane-impermeable calcium indicator, Calcium Green-5N, to indicate the Ca^{2+} signal change. Mitochondria have the ability to uptake Ca^{2+} ions until the Ca^{2+} concentration reaches a limit past which Ca^{2+} ions will then be released through the opening of the permeability transition pore (PTP). In the current study and in agreement with our previous reports (*27*, *28*), we measured a significantly reduced capacity of CRC in both *Sod1*KO and aging muscles compared to WT muscles (Fig. 7, A and B). The mitochondrial respiratory functions measured using respirometry in permeabilized muscle fibers show both reduced oxygen consumption rate (OCR) upon the addition of different substrates to stimulating electron flow through different complexes (I, I + II, II, and IV) and elevated reactive oxygen species (ROS) production rate in state 1 respiration (mitochondria respiring without addition of external substrate; Fig. 7, C and D).

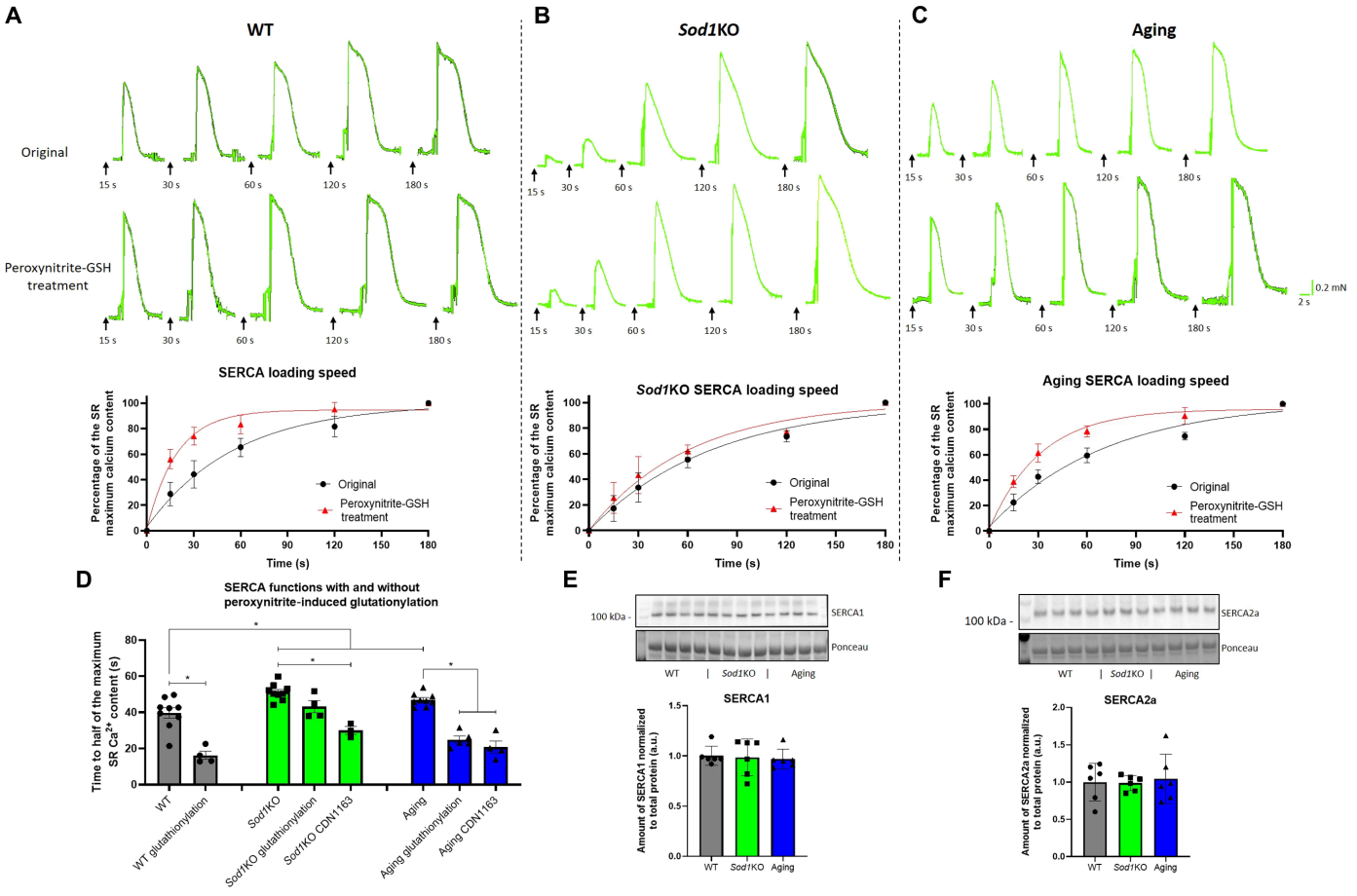

Fig. 5. Relative SERCA activity in single skinned fast-twitch muscle fibers before and after peroxynitrite-induced glutathionylation, along with the relative protein amount of SERCA in muscle homogenates. Through reloading SR for different periods of time and depleting SR Ca^{2+} storage, SERCA activity can be measured in single skinned fibers as described in Materials and Methods. Peroxynitrite-GSH treatment was applied on the same fiber after the original sequence of SR repletion and depletion to show the effect of glutathionylation on SERCA activity. CDN1163 treatment was applied on *Sod1*KO and aging muscle fibers as a positive control of the increasing potential of SERCA activity. (**A** to **C**) Representative force traces of the force response upon the SR depletion after each different loading time in single fast-twitch fibers from WT, *Sod1*KO, and aging mice, along with the pooled force–loading time curve for each group. (**D**) Pooled data of loading time to half of the maximum SR Ca^{2+} content for individual muscle fibers in different groups with and without glutathionylation, as well as with the CDN1163 treatment in *Sod1*KO and aging groups. (**E** and **F**) Representative Western blot images with pooled data showing the protein amount of SERCA1 and SERCA2a in GTN muscle homogenates. *Significant difference between labeled groups ($P < 0.05$, one-way ANOVA). For the SERCA activity data, $n = 3$ to 9 indicates the number of fibers analyzed, and $N = 3$ to 4 indicates the number of animals from which the fibers were obtained; for the SERCA amount in Western blotting, $n = 6$ indicates the number of animals. Data are presented as means ± SD.

DISCUSSION

Similar to loss of muscle mass, a reduction in muscle strength is a critical component of health span in aging, yet the underlying causes are still not completely established. In particular, the impact of aging and, more specifically, elevated oxidative stress on the specific components involved in E-C coupling are not well defined. Our study directly measured the effects of aging and elevated oxidative stress on the regulation of E-C coupling components, including membrane excitability, contractile filament function and Ca^{2+} sensitivity, Ca^{2+} release, reuptake and SR Ca^{2+} storage, and downstream changes in mitochondrial Ca^{2+} buffering capacity and function. In aged WT mice and a mouse model of elevated oxidative stress (*Sod1*KO mice), we found a comparable reduction in specific force production in whole GTN in old mice and adult *Sod1*KO mice in situ, associated with NMJ impairments and similar impairments in mitochondrial calcium buffering capacity and mitochondrial function. In contrast, in isolated skinned fibers from old mice, specific force generation, cross-bridge ATPase activity, and membrane excitability are not impaired, while fibers from adult *Sod1*KO mice continue to show significant deficits in these parameters. Myofibrillar calcium sensitivity calcium storage and SERCA ATPase activity are impaired in isolated fibers by both aging and oxidative stress to a similar degree. SERCA activity can be activated by glutathionylation in fibers from the aged mice, while fibers from *Sod1*KO mice are resistant to activation, suggesting irreversible oxidative damage to the SERCA ATPase protein in *Sod1*KO fibers. These findings are important, as they indicate a differential susceptibility of molecules or structural components within the E-C coupling system to oxidative stress and aging that may be related to the underlying mechanisms of sarcopenia.

In agreement with our previous findings (*1*, *15*), the results presented here clearly confirm that both *Sod1*KO and aging mice exhibit significant muscle weakness associated with a disruption of NMJ morphology and function at the whole muscle level. In contrast,

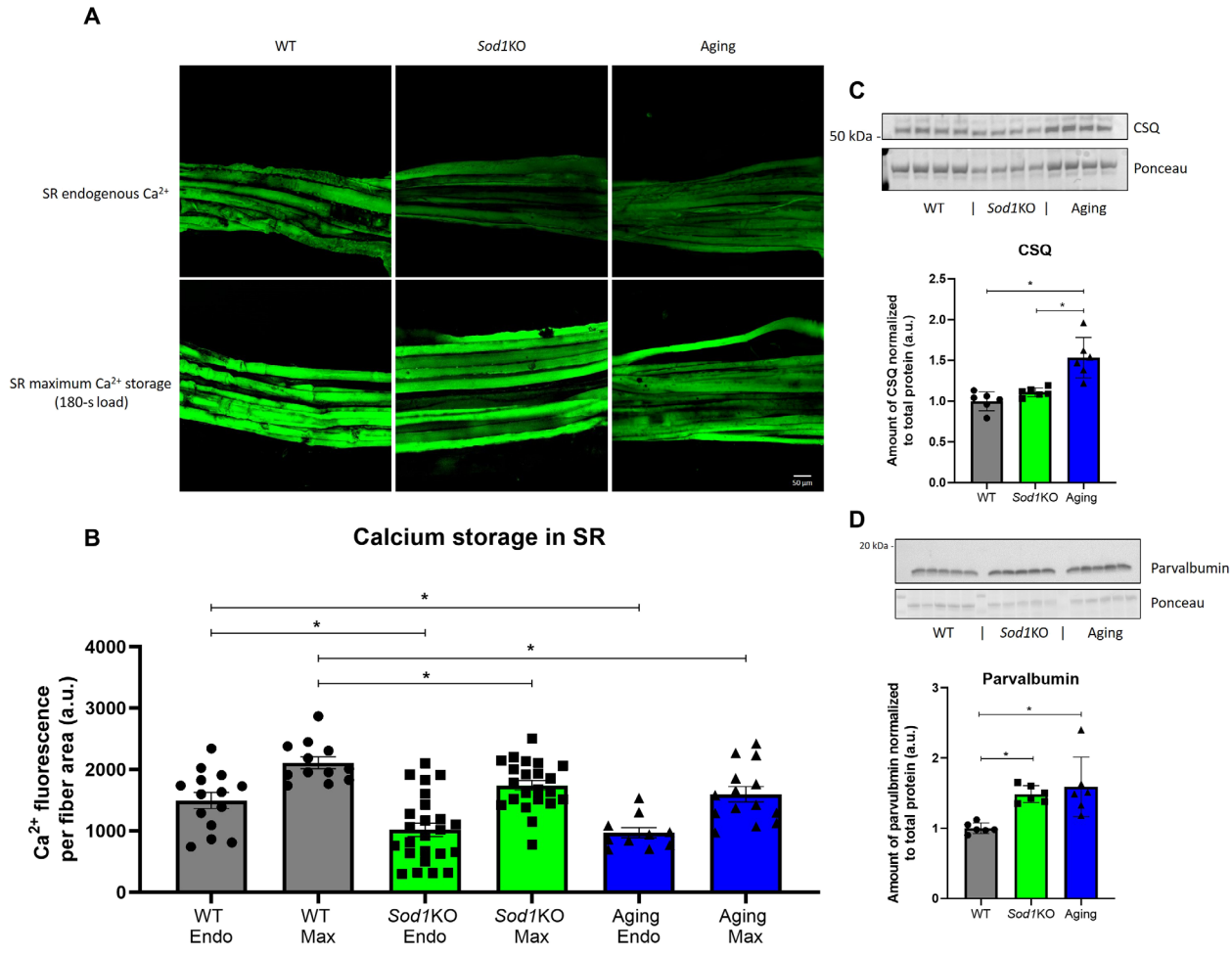

Fig. 6. Endogenous and the maximum Ca^{2+} storage in SR and the relative amount of calcium storing and transporting proteins in muscle homogenates. Chemically permeabilized muscle fiber bundles were stained using Fluro-5F fluorescent dye at both the SR endogenous Ca^{2+} storage level and the maximum Ca^{2+} storage level (180 s in loading solution). Then, the fluorescent images were taken using the confocal microscope under the same magnification and fluorescence intensity. *Z*-stacks were taken to include all Ca^{2+} signals from the 3D structure of intact fiber. (**A**) Representative confocal images of Ca^{2+} fluorescent signals in fiber bundles from different groups at SR endogenous and maximum Ca^{2+} storage levels. (**B**) Pooled data showing the Ca^{2+} fluorescence densitometry at a given fiber area in different groups at endogenous and maximum SR Ca^{2+} storage levels. (**C** and **D**) Representative Western blot images with pooled data showing the relative amount of CSQ and parvalbumin in muscle homogenates from WT, *Sod1*KO, and aging mice. *Significant difference between labeled groups ($P < 0.05$, one-way ANOVA). For the Ca^{2+} storage data, $n = 10$ to 22 indicates the number of fiber bundles analyzed, and $N = 3$ indicates the number of animals from which the fiber bundles were obtained; for the protein amount in Western blotting, $n = 6$ indicates the number of animals. Data are presented as means ± SD.

when contractile function is measured at the single fiber level by direct maximum Ca^{2+} activation, thereby removing extrinsic factors such as signal transmission though the NMJ, there is no longer a deficit in force generation in fibers from the aging mice compared to young WT mice, while the fibers from the *Sod1*KO mice still showed significant weakness at the single fiber level. To further investigate this difference, we measured the ATPase activity of the fiber cross-bridges where the interaction of myosin and actin generates muscle force (*29*). Consistent with the single fiber force generation, the cross-bridge ATPase activity is also decreased in *Sod1*KO fibers compared to young WT fibers, while no reduction is observed in the aging muscles. These findings are important and support the conclusion that elevated oxidative stress impairs force generation at the single fiber level, while aging does not have this effect. The reduction in force generation that we measure at the whole muscle level is due to both intrinsic properties of the fibers and contractile proteins and factors outside the properties of the fibers themselves, such as transmission of electrical nerve stimulation through the NMJ; calcium kinetics and homeostasis in the muscle tissue; and other factors related to muscle quality such as metabolism, fibrosis, and lipid content. Although *Sod1*KO and aging mice share an equivalent extent of muscle weakness at whole muscle level, there are differences in the underlying mechanisms responsible for the weakness in these two models. Because in situ electrical stimulation applies the electrical stimulus onto the nerve or muscle surface directly to generate action potentials that initiate E-C coupling events and force generation (*17*) while force at the single fiber level by direct maximum Ca^{2+} activation is generated directly from the cross-bridge and contractile filaments independent of other E-C coupling components (*30*), our results suggest

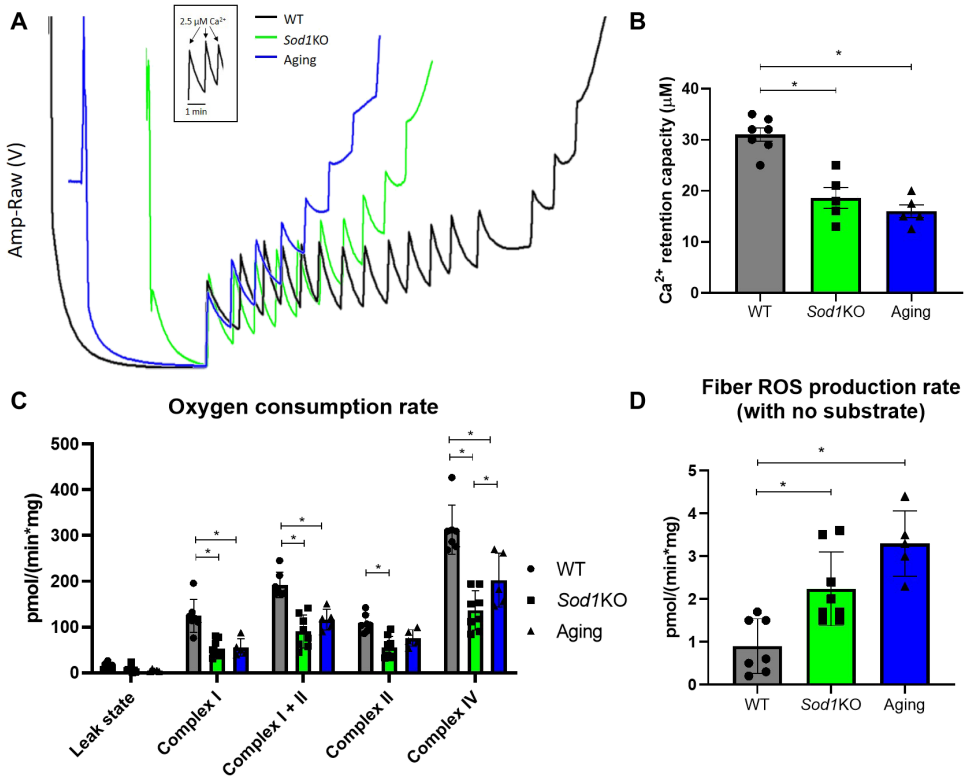

Fig. 7. Detection of mitochondrial CRC and respiratory functions. Mitochondrial CRC was measured in isolated mitochondria from GTN muscle through the addition of sequential calcium ions (2.5 μM every 1 min), and the membrane-impermeable calcium indicator, Calcium Green-5N was applied to indicate the Ca^{2+} signal change. Respiratory functions measured with Oxygraph-2k technique using permeabilized muscle fibers from GTN muscle. (**A**) Representative calcium signal trace of mitochondrial CRC in isolated mitochondria from WT, *Sod1*KO, and aging muscles. (**B**) Quantified mitochondrial CRC across different groups. (**C**) Respiratory rate or OCR (for the rate of oxidation phosphorylation) of mitochondria in permeabilized muscle fibers. Substrates used for different complexes added sequentially. Leak state, 10 mM glutamate and 2 mM malate with no adenosine diphosphate (ADP); complex I, addition of 2.5 mM ADP; complex I + II, addition of 10 mM succinate; complex II, addition of 0.5 μM rotenone; complex IV, addition of 2 mM ascorbate and 0.5 mM TMPD added after 5 μM antimycin A. (**D**) ROS production rate of permeabilized muscle fibers with no substrate. *Significant difference between labeled groups ($P < 0.05$, one-way ANOVA). For the mitochondrial CRC detection, $n = 5$ to 7 indicates the number of animals, and for the mitochondrial function assay (including OCR and ROS), $n = 5$ to 8 indicates the number of animals. Data are presented as means ± SD.

that the weakness seen at the whole muscle level in aging muscle is due to impairments preceding the E-C coupling process rather than the impairment of contractile filaments or cross-bridges.

One step preceding the cross-bridge force-generating process is Ca^{2+} sensing and binding to troponins on contractile filaments. If fiber Ca^{2+} sensitivity is changed, then the final force output will also be altered (*19*). In this study, we measured the Ca^{2+} sensitivity of fiber contractile filaments in single skinned fast-twitch fibers and found a similar decrease in both *Sod1*KO and aging fibers compared to WT fibers. This result suggests that the muscles from both *Sod1*KO and aging mice are less sensitive to Ca^{2+} signals and thus will generate less force than young WT muscle in response to the same Ca^{2+} concentration and will require a higher Ca^{2+} concentration to achieve the same force production that fibers from WT muscle produce at a lower Ca^{2+} concentration. However, under physiological conditions, the peak of intracellular Ca^{2+} transient following each action potential is regulated in mammalian muscle cells to avoid the high Ca^{2+} concentration used to activate the maximum force in our experimental protocol (*31*). This is critical to muscle health as high Ca^{2+} concentration can be detrimental to muscle cells through activation of multiple protein degradation pathways.

It has previously been reported that fast-twitch muscle fibers can increase Ca^{2+} sensitivity through a reversible *S*-glutathionylation of the TnI Cys^{134} residue. The thiol group on Cys residues is a key target for oxidative modification of proteins. Reaction with glutathione induces protein *S*-glutathionylation that is an important oxidative mechanism for regulating critical cellular processes. For example, as described by Araki *et al.* (*32*), highly reactive thiols are a key regulator of specific, rapid cellular signaling changes that support cellular function (*32*). *S*-glutathionylation in skeletal muscle is an adaptive process that occurs after exercise to increase fiber sensitivity to Ca^{2+} ions, which will support a demand for higher force output without requiring high levels of Ca^{2+}. This is a beneficial and protective mechanism for muscle cells (*19*, *22*, *33*). To elicit *S*-glutathionylation under experimental conditions in vitro, fast-twitch muscle fibers are exposed to sulfhydryl-specific oxidant, DTDP, and GSH, resulting in a significant increase in fiber Ca^{2+} sensitivity (*19*). In the current study, we adopted this protocol to treat fast-twitch fibers from WT, *Sod1*KO, and aging muscles. We measured an increase in Ca^{2+} sensitivity in WT fibers in agreement with previously reported results (*20*). We observed an increase in Ca^{2+} sensitivity in both *Sod1*KO and aging fibers that was blunted compared to the response measured following *S*-glutathionylation in WT

fibers. This suggests that the TnI Cys^{134} residue is less responsive to *S*-glutathionylation in muscles from *Sod1*KO and aging mice; however, the exact mechanism responsible is not fully understood. TnI is known to be susceptible to oxidative damage, and irreversible oxidative modifications on TnI will result in either the prevention of the formation of *S*-glutathionylation on the Cys^{134} residue or a blunted increase in Ca^{2+} sensitivity produced by *S*-glutathionylation (*20*, *34*). Both *Sod1*KO and aging mouse models are known to have high oxidative stress in their skeletal muscles (*1*, *10*). It is possible that a high oxidative stress environment impairs the regulatory effects of TnI on muscle physiological function and muscle performance. In *Sod1*KO and aging fibers, a blunted Ca^{2+} sensitivity and impaired reaction to *S*-glutathionylation are potentially deleterious to muscle cells, leading to an intracellular environment exposed to a higher Ca^{2+} concentration after contraction, impaired Ca^{2+} homeostasis, and further damage to the cell through activation of degradation pathways (*35*, *36*). Thus, our results showing blunted calcium sensitivity in aging and *Sod1*KO fibers, although small in magnitude, are physiologically very important because of the need to tightly control calcium homeostasis and avoid the need for elevated calcium levels that can be harmful. A report by Lamboley *et al.* (*20*) found changes of a similar magnitude in older human subjects, which led to a significant force deficit.

Excitation is a key player in force production and output. A properly polarized membrane and t-tubule system are pivotal for conductance of the action potential. In contrast, a poorly polarized membrane will result in the inactivation of the voltage sensors in the t-system impairing Ca^{2+} release and reducing contractile force generation (*37*). In the current study, we measured the membrane excitability in fast-twitch fibers by depolarizing the t-system via ionic substitution as previously reported (*21*, *22*). A healthy fiber produces as high as 80% of its maximum Ca^{2+}-activated force (*22*). We found that membrane excitability is extremely poor in *Sod1*KO fibers, and aging fibers, while better than *Sod1*KO fibers, are still less active than WT fibers. Thus, impaired membrane polarization and excitability in *Sod1*KO and aging mice may impair depolarization and activation of the voltage sensors and reduce force generation and are consistent with a lack of impairment in the aging fibers that do not contain intact membrane structures. There are many factors that can affect muscle membrane excitability. Among them, NKA is the key enzyme governing the resting polarization status and the rapid repolarization process of the t-system, and its amount and activity are subject to change with external alterations, such as exercise or aging (*22*, *38*–*40*). There are two main subunits that comprise the NKA enzyme, NKAα and NKAβ, and NKAα is the catalytic subunit. For NKAα, there are two different isoforms: NKAα1, which is the ubiquitous isoform appearing in all cell types, and NKAα2, which is expressed specifically in muscle cells. On the basis of Western blotting data, we observed a significant decrease in the amount of NKAα2, the muscle-specific isoform, in muscles from *Sod1*KO and aging mice. This decrease in NKAα2 supports the poor membrane excitability seen in the fiber experiments. The magnitude of the reduction in NKAα2 in both models, the fact that NKAα2 is slightly higher in aging fibers, and the fact that the ubiquitous NKAα1 isoform is decreased only in *Sod1*KO muscles all support the reduced membrane excitability in these models and the slightly better excitability in aging muscle compared to the *Sod1*KO muscle. The specific relationships between NKA and oxidative stress are still not fully understood, and a recent study suggests that NKA signaling might not be the result of oxidative stress but rather the reason for the high oxidative stress (*40*). In addition to its well-known function as an ion pump, studies in obesity and cardiovascular disease suggest that NKA also has a signaling function that can exacerbate oxidative stress by activating signaling cascade pathways that lead to the production of even excessive mitochondrial ROS (*41*, *42*).

In response to a membrane action potential, Ca^{2+} release is triggered through an interaction between voltage sensors (DHPR) on the t-tubule system and the calcium release channels RyR on SR (*14*). In general, we did not observe a change in the content of DHPR and RyR across all three groups. However, we did notice a decreased amount of calstabin, the stabilizing protein of RyR channel, in *Sod1*KO and aging muscles. This reduction was previously reported by our group, suggesting that the RyR structures may not be stable in the muscles from these two groups, possibly leading to RyR malfunctions or, potentially, Ca^{2+} leakage (*1*). In the face of these changes in RyR, membrane depolarization in response to Ca^{2+} release may not reach a level in *Sod1*KO and aging muscles great enough to support force production measured in situ at the whole muscle level.

During the E-C coupling process, Ca^{2+} ions act as a messenger playing a critical role in converting electrical signals into a muscle twitch. For this reason, regulating Ca^{2+} ions and maintaining proper Ca^{2+} homeostasis in the muscle cell are important for proper muscle function. In muscle cells, SERCA is the key regulator of intracellular Ca^{2+} concentration, pumping Ca^{2+} back into the SR lumen after each twitch to maintain the intracellular Ca^{2+} concentration at a very low level (~20 to 50 nM) (*43*). In the current study, using skinned single fibers exposed to depletion and repletion of SR Ca^{2+} storage, we also found a reduction in SERCA activity in fast-twitch fibers from *Sod1*KO and aging muscles. This reduction is similar in magnitude to our previous studies in *Sod1*KO and aging muscles in which SERCA activity was measured with muscle homogenates (*15*, *16*, *44*). Furthermore, similar reductions of SERCA activity have been reported in other models of muscle dysfunction including the mdx mouse model of muscular dystrophy and in muscle from older asthma patients (*45*), supporting the physiologic importance of SERCA activity in muscle in aging and disease. This reduction is not due to a change in the level of SERCA protein. The underlying mechanism for the oxidative stress–induced decrease in SERCA activity has been elucidated and is predominantly attributed to oxidative damage to the Cys^{674} residue of SERCA (*23*–*26*). If the Cys^{674} residue is damaged by elevated oxidative stress, SERCA activity is markedly decreased. The Cys^{674} residue is involved in redox regulation of SERCA activity, enhancing SERCA activity through peroxynitrite-induced reversible *S*-glutathionylation under physiological conditions. Studies defining the regulation of SERCA activity using reconstituted SERCA molecules were previously reported (*23*). However, the regulatory function of Cys^{674} in living muscle cells with native SERCA protein has not been conducted. Here, we tested the regulation of Cys^{674} in living muscle fibers by *S*-glutathionylation of the Cys^{674} residues of native SERCA, induced by peroxynitrite-GSH treatment to mimic actual physiological conditions. After *S*-glutathionylation, we found a significant increase in SERCA activity in both young WT and aging fibers, suggesting that the regulatory function of the Cys^{674} residue in SERCA from these two groups is intact, although the increased amount in aging fibers is slightly smaller than in young WT fibers. However, there is no response detected in *Sod1*KO fibers after the *S*-glutathionylation.

We hypothesized that the resistance to activation of SERCA after the *S*-glutathionylation treatment in *Sod1*KO fibers was related to the Cys^{674} site. To test this, we used a proven allosteric SERCA activator, CDN1163 (*16*, *44*, *46*), to treat the same fiber again and found a significant increase of the SERCA activity, indicating that SERCA can be activated allosterically. Therefore, the lack of SERCA activation after the *S*-glutathionylation treatment in *Sod1*KO fibers suggests that either there is damage on their Cys^{674} residues or the sites of *S*-glutathionylation on Cys^{674} residues are occupied or impaired by oxidative modifications.

As our group reported previously, if SERCA activity is reduced, then there may be a dysregulation of Ca^{2+} homeostasis in the cytosol and SR lumen that can alter the amount of some Ca^{2+} handling marker proteins, such as CSQ and parvalbumin (*1*, *15*). In agreement with our previous findings, parvalbumin levels are increased to regulate the cytosolic Ca^{2+} concentration by transporting Ca^{2+} ions to SERCA. Previous studies have shown that the increased level of parvalbumin reflects an abnormally high cytosolic Ca^{2+} concentration (*47*). We noticed the increase in the amount of CSQ in aging muscles again but not in *Sod1*KO muscles. This is possibly due to an adaptive alteration in aging muscles in which the RyR may be somewhat leaky. In addition, if SERCA activity is low, then the SR may accumulate more CSQ to store more Ca^{2+} ions to meet the high demand of Ca^{2+} ions during a muscle twitch. However, this does not explain why CSQ content in *Sod1*KO muscles is not similarly elevated despite a larger effect on the RyR and SERCA activity. One potential explanation may be an induction of tubular aggregates in the SR that tend to accumulate more CSQ, as occurs in the arrays of elongated SR tubules in skeletal muscles from patients with aging-induced myopathies (*48*). Although CSQ is increased in aging muscles, we actually detected a reduced Ca^{2+} storage in the SR based on staining in fiber bundles at both endogenous and maximum loaded levels in both aging and *Sod1*KO muscles compared to WT controls. This result is consistent with a previous study reporting decreased SR Ca^{2+} content at both endogenous and maximal levels in aged human muscles (*20*). Two decades earlier, it was reported that the peak of the intracellular Ca^{2+} transient to depolarization was ~30% lower in fibers of old subjects than in young subjects. This phenomenon was putatively attributed to the "finite level" of Ca^{2+} storage at the point of peak release (*49*). SR Ca^{2+} storage is decided by many factors, and an increase in Ca^{2+} leakage of the SR, which is sensitive to oxidative stress, is considered as a likely cause of the lower Ca^{2+} content in the SR in aged muscles. For example, Andersson *et al.* (*50*) reported an age-related oxidation of RyR in skeletal muscle in older mice, which resulted in an intracellular Ca^{2+} leak that could be reduced by treatment of the mice with a compound, S107, that stabilized the binding of calstabin to RyR. Muscle force was also enhanced markedly. These findings strongly support our results, as we also noticed a markedly reduced amount of calstabin in *Sod1*KO and aging muscles, which potentially induce the instability of RyR and cause the leakage of Ca^{2+} from SR and therefore result in a lower SR Ca^{2+} content.

Other than the SR, mitochondria are another important cellular Ca^{2+} buffering pool in cytosol, and maintenance of mitochondrial function requires proper Ca^{2+} metabolism. Dysregulation of Ca^{2+} dynamics in mitochondria or impairment of cellular Ca^{2+} homeostasis will incur abnormal mitochondrial function, cell damage, or even cell death (*51*). Our data suggest impairments in Ca^{2+} regulation affecting several sites, including the RyR, parvalbumin, SERCA, and SR, in *Sod1*KO and aging muscles. Therefore, we asked whether cellular Ca^{2+} homeostasis was disturbed in muscle from these two models and whether there was an impact on mitochondrial Ca^{2+} metabolism or respiration. To test this, we challenged the mitochondrial CRC in isolated mitochondria from muscles in all three groups as previously described (*4*, *27*). We observed a significant decrease in CRC in mitochondria from both *Sod1*KO and aging muscles compared to WT muscles, indicating a significant impairment in mitochondrial Ca^{2+} buffering capacity, which is similar to what Picard *et al.* (*52*) reported in aging muscles from rats. In addition, using permeabilized muscle fibers, we found impaired mitochondrial function (reduced OCR and increased ROS production) in muscle from *Sod1*KO and aging mice in agreement with our previous studies (*9*, *15*). Last, as we recently proposed (*46*), the impaired mitochondrial function supports a potential for elevated oxidative stress in skeletal muscle cells, which can lead to oxidation and modification of Ca^{2+} regulating sites (i.e., RyR and SERCA) and other molecules associated with E-C coupling (i.e., TnI and NKA) and force generation. In turn, oxidative modifications on these Ca^{2+} regulating sites may dysregulate cellular Ca^{2+} homeostasis, further leading to elevated cytosolic Ca^{2+} concentration, and thus further impair mitochondrial functions, generating a vicious cycle. Therefore, targeting on the Ca^{2+} regulating sites to break the cycle may be a strong potential strategy for future studies, possibly even more effective than only targeting on mitochondria.

In summary, this study demonstrates the impact of aging and oxidative stress on E-C coupling and Ca^{2+} regulating systems in skeletal muscle cells. Our results clearly show a loss of muscle strength in these two models, potentially caused by decreased Ca^{2+} sensitivity of contractile filaments, damaged TnI, reduced membrane excitability with altered NKA signaling and RyR stability, suppressed SERCA activity via modification of the Cys^{674} residue on the SERCA protein, lowered SR Ca^{2+} storage and increased cytosolic Ca^{2+} concentration, and lastly impaired mitochondrial Ca^{2+} metabolism and respiratory functions. This study also confirms the differences between *Sod1*KO and aging models and analyzed the underlying mechanisms. Last, this study elucidates a vicious cycle with revealing the cross-talk among oxidative stress, Ca^{2+} homeostasis, and force generation. Together, these specific findings provide a comprehensive knowledge toward a better understanding of muscle weakness in aging and also shed light on the future developments of interventions on some new targets for countering muscle weakness and the high oxidative stress in aged muscles.

MATERIALS AND METHODS

Animals and the generation of the whole-body *CuZnSod* knockout (*Sod1*KO) mice

The mice used in this study were maintained on a C57BL/6J background. The *Sod1*KO mice were originally generated by C. Epstein's laboratory at the University of California San Francisco, and the details have been previously reported (*10*, *53*). All mice were caged in a pathogen-free environment with free access to standard chow and water and maintained on a 12-hour light/dark cycle. Only female mice were used in this study, and measurements were done at 12 months of age in WT and *Sod1*KO mice and at 24 months of age in aged WT (aging) mice, unless otherwise stated. The Institutional Animal Care and Use Committee at Oklahoma Medical Research Foundation (Oklahoma City, OK, USA) approved all procedures.

Assessment of muscle contractile properties and NMJ functions

On the basis of the methods that we described previously, the isometric contractile force generation was measured with in situ electrical stimulation in GTN muscle (*15*, *17*). Briefly, mice were anesthetized with isoflurane, and the whole GTN muscle was cleaned and isolated from surrounding muscles and connective tissues. After the isolation, the muscle was tied with silk suture on the distal tendon, and then, the tendon was severed and mounted onto the force transducer (model 305B, Aurora Scientific). A temperature-controlled platform at 37°C was used for maintaining the body temperature, and the mouse was provided with continuous anesthesia. The electrode was placed on the surface of GTN muscle directly, and the optimal length of the muscle was adjusted with single 0.2-ms stimulation pulses until a maximum twitch was reached. At the muscle optimal length, a series of 300-ms stimulus pulses were applied to achieve the maximum isometric tetanic force. After the muscle stimulation, the electrode was moved from muscle to the sciatic nerve, and the nerve filament was hooked firmly. Then, the same pulses of tetanic stimulus were applied to the sciatic nerve to achieve the nerve-induced maximum isometric tetanic force. All of the above tetanic twitch protocols were repeated several times to confirm the reproducibility and reliability of the data.

After the force measurements were completed, muscles were carefully removed and weighed, and the specific maximum tetanic force was derived by normalizing the maximum force production to the muscle cross-sectional area calculated by the length and weight of the GTN muscle [dividing the muscle mass (in mg) by the optimal length (in mm) and the density of mammalian skeletal muscle (1.06 g/cm^3)] to give the specific force (in N/cm^2). The NMJ function was presented by normalizing the nerve-induced force to the muscle-induced force as a percentage.

Cross-bridge ATPase activity assay

Cross-bridge ATPase activity was measured with extracted MHCs from GTN muscle homogenates as described previously (*29*). Briefly, MHC was extracted by homogenizing GTN muscle samples with high salt buffer, containing 300 mM NaCl, 1 mM EGTA, 3 mM $MgCl_2$, and 5 mM Hepes. After homogenization, the samples were centrifuged at 15,000*g* or 10 min at 4°C, and the supernatant was collected. Protein content was then detected with Bradford assay, and 100 μg of protein was added into 10 ml of reaction buffer, including low Ca^{2+} buffer (containing 90 mM Hepes, 50 mM EGTA, and 4 mM $MgCl_2$) for detecting the ATPase activity at the resting status and high Ca^{2+} buffer (containing 90 mM Hepes, 3 mM $CaCl_2$, and 4 mM $MgCl_2$) for the Ca^{2+}-activated status. The reaction was initiated by adding 5 mM adenosine triphosphate (ATP) into the system, for 30 min at room temperature, and then quenched by adding 34% citrate. Colorimetric solution was prepared by mixing 0.045% malachite green (MG) and 4.2% ammonium molybdate (AM; in 4 M of HCl) following the ratio 3:1 (MG/AM mixture). Samples from the reaction system along with a rage of PO_4^{3-} (P_i) standard solutions (between 0 and 160 μM) were added into the MG/AM mixture with the ratio 1:5 (i.e., 40 μl into 200 μl); then, this new mixture was loaded in to the 96-well plate, and the absorbance rate was read at 660 nm. Last, the free amount of P_i in each sample can then be determined on the basis of the standard solutions, and the final ATPase activity can be calculated with the following equation

$$\frac{[PO_4^{3-}]\ \mu M \times 10\ ml}{30\ min \times 100\ \mu g\ protein} = n\ \mu mol\ P_i/min/mg\ protein$$

Single muscle fiber dissection and buffers used in single fiber manipulations

After mice were euthanized, extensor digitorum longus (EDL) muscle was excised from each animal and used for obtaining single skinned fast-twitch muscle fiber segments. As described previously (*22*), after the muscle dissection, EDL muscle was pinned at resting length at room temperature under the paraffin oil on a SYLGARD layer and kept cool on an ice pack (~10°C). Single muscle fiber segments were dissected under a light microscope, and the sarcolemma was removed by mechanically skinning the fiber segment using fine forceps, as described previously. Then, the skinned fiber segment was mounted onto the muscle-station-skinned (MyoTronic, Heidelberg, Germany) at the resting length (i.e., length just less than that eliciting measurable passive force), between the forceps and transducer (TR5S, MyoTronic) provided with the station. Sarcomere length was then measured at the beginning by the laser diffractions provided with the station following the mechanisms described before (*54*), and there is no difference observed across three different groups (all sarcomere lengths are around 2.5 μm). At the end of experiment, fiber type of each skinned single fiber was ascertained by exposing it to a strontium solution at pSr 5.2; type II fibers produce very little force at pSr 5.2, whereas type I fibers produce >80% of the maximum force (*21*, *22*, *55*). All fibers examined in this study were fast-twitch fibers unless otherwise stated. Fibers used for single fiber analysis will be primarily type IIB fibers, as the EDL muscle is composed of predominantly fast-twitch fibers. In addition, type IIB fibers are the largest in size and will be preferentially represented in single fiber analysis.

All chemicals used for single fiber manipulations were from Sigma-Aldrich (St. Louis, MO, USA) unless otherwise stated. Two heavily Ca^{2+}-buffered solutions were used for examining the properties of the contractile apparatus: "relaxing solution," containing 126 mM K^+, 36 mM Na^+, 1 mM free Mg^{2+} (10.3 mM total Mg^{2+}), 90 mM Hepes, 50 mM EGTA, 8 mM ATP, 10 mM creatine phosphate (pH 7.10), pCa (= $-\log10[Ca^{2+}]$) > 9, and an osmolality of 295 ± 10 mosm/kg H_2O and "maximal Ca^{2+}-activating solution," which was very similar but with 50 mM CaEGTA (at pCa ~ 4.7) instead of EGTA and with 8.1 total Mg^{2+} to keep the free [Mg^{2+}] at 1 mM (*21*, *22*, *55*). For assessing fiber type as mentioned above, a strontium-based solution at pSr 5.2 was made similarly to maximal Ca^{2+}-activating solution but with Sr^{2+} instead of Ca^{2+} and mixing this with relaxing solution at ratio of 1:7. K-HDTA solution was used to examine excitation-contraction coupling (membrane excitability) and SERCA properties; it was similar to relaxing solution but with HDTA replacing EGTA and contained 126 mM K^+, 36 mM Na^+, 1 mM free Mg^{2+} (8.5 mM total Mg^{2+}), 90 mM Hepes, 50 mM HDTA, 0.05 mM EGTA, 8 mM ATP, and 10 mM creatine phosphate (pH 7.10), with the free [Ca^{2+}] weakly buffered at pCa ~ 7.1, and an osmolality of 295 ± 10 mosm/kg H_2O. In addition, a Na-HDTA solution was made similarly to the K-HDTA solution by substituting all K^+ with Na^+, which was achieved by adjusting pH with NaOH instead of KOH. Na-HDTA solution was used to depolarize the t-tubules in skinned muscle fibers.

Single skinned fiber manipulation

Measurement of contractile apparatus parameters (maximum specific force and calcium sensitivity)

Fiber cross-sectional area (in mm^2) was calculated by measuring the fiber diameter in three different places along the length of the fiber, as described previously (*21*, *22*). The maximum specific force (in mN/mm^2) was calculated by normalizing the maximum Ca^{2+}-activated force of the fiber to its cross-sectional area. After mounting onto the transducer and measurement of the sarcomere length as described above, the fiber was then stretched to 120% of its resting length and transferred into a Perspex bath containing 2 ml of relaxing solution for 2 min and then activated in a sequence of solutions with progressively higher levels of free [Ca^{2+}] (pCa ~ 9 to 4.7), with maximum force produced at pCa 4.7 (*21*, *22*). Force was recorded with a bridge amplifier (MyoTronic) and the Aurora Data Acquisition Signal Interface (604A) with DMC software (Aurora, ON, Canada). After going through the sequence, the fiber was then moved back into relaxing solution where it fully relaxed again. Such force-pCa staircases were repeated two to three times for each fiber. The force at each [Ca^{2+}] within a given sequence was expressed as a percentage of the corresponding maximum force, and the data were fitted with a Hill curve, using GraphPad Prism 9 software, to ascertain values of pCa50 (pCa at half of the maximum force production) indicating the Ca^{2+} sensitivity of contractile apparatus.

To induce *S*-glutathionylation on TnI, a DTDP-GSH treatment was applied to the fibers. GSH was made in K-HDTA solution as 100 mM stock and then diluted 20-fold to give 5 mM in the final solution. DTDP was made in absolute ethanol at the concentration of 100 mM and diluted 1000-fold in the final solution to 100 μM; such amount of ethanol (0.1%) had no noticeably different effect from controls without ethanol (*19*). Briefly, after the test of force-pCa staircases, fibers were treated with 100 μM DTDP for 5 min and then treated with 5 mM GSH for 2 min. Soon after the treatment, the fiber underwent the force-pCa test again, and then, the pCa50 values were calculated again upon the new staircases to compare with the old values before the treatment.

Measurement of membrane excitability

Membrane excitability was also examined in skinned single fast-twitch fibers, through the detection of depolarization-induced force responses. When a muscle fiber is mechanically skinned, the t-system seals off, and if the skinned fiber segment is placed in the standard K-HDTA solution, then it can become polarized again because the action of the Na-K-ATPase (Na-K pump, NKA) in the t-system membrane establishes a high sodium ion concentration and a low potassium ion concentration within the t-system (*14*). If the t-system is sufficiently well polarized, then the voltage sensors (DHPRs) in the t-system return to an activatable state (*56*), and if the skinned fiber is subsequently transferred into the zero potassium (Na-HDTA) solution, then the t-system is rapidly depolarized, activating the voltage sensors, which, in turn, trigger Ca^{2+} release from the SR and a resultant force response (*14*). Thus, the magnitude of the depolarization-induced response in a skinned fiber (relative to the maximum Ca^{2+}-activated force in that fiber) can be used as a measure of the polarization of the t-system membrane and excitability of that fiber. We have previously shown that maximal depolarization-induced responses can readily be elicited in skinned fast-twitch fibers from EDL muscle, while the responses in slow-twitch fibers were much poorer (*21*). In this study, through the ionic substitution from K^+ to Na^+, we measured the depolarization-induced responses of fast-twitch fibers from all three different groups.

Detection of SERCA activity in single skinned fibers

SERCA activity was measured in single skinned fast-twitch fibers through depletion and repletion of the SR Ca^{2+} storage. The skinned fiber segment was placed in weakly buffered K-HDTA solution, and first, its Ca^{2+} storage was completely emptied by exposure of the fiber to a K-HDTA solution with low free [Mg^{2+}] and 30 mM caffeine (full release solution). Then, the SR was "reloaded" with Ca^{2+} by placing the fiber in a loading solution (K-HDTA solution with 1 mM total EGTA at pCa 6.7) for a different period of time, i.e., 15, 30, 60, 120, and 180 s. After the SR was reloaded at each time period, the fiber was then exposed to the "full release solution" again to empty the loaded Ca^{2+}, and the released Ca^{2+} upon depletion will then trigger a force response. The time integral (area) of the force response to the exposure to the "full release" solution was indicative of the loaded SR Ca^{2+} content. Through normalizing the area of force responses at each loading time period to the maximum loading time at 180 s as a percentage, we were then able to plot a time–SR Ca^{2+} content curve, and on the basis of this curve, the "time to half of the maximum load" can be calculated and used to indicate SERCA activity in the fibers.

It is known that physiologically, SERCA reversibly regulates its activity through peroxynitrite-induced *S*-glutathionylation on its Cys^{674} residue, with the activity being markedly increased after the *S*-glutathionylation (*23*, *25*). To reproduce this physiological process in skinned muscle fibers, we used peroxynitrite-GSH treatment to induce this *S*-glutathionylation on the Cys^{674} residue on SERCA, where we first treated the skinned fiber segment with 100 μM peroxynitrite for 5 min and then moved the fiber to 100 mM GSH for 2 min in K-HDTA solution. After the treatment, the fiber was then moved back to undergo the SR depletion and repletion process for measuring the SERCA activity. We observed a significant increase in SERCA activity in WT fibers after the treatment, and this effect is reversible by treatment with 10 mM DTT (10 min) in K-HDTA solution (fig. S3), indicating that this experimental peroxynitrite-induced *S*-glutathionylation is similar to what is happening in vivo. At the end of each experiment, some fibers were further treated with CDN1163 (200 μM CDN1163 in K-HDTA solution for 10 min) and tested the SERCA activity again. CDN1163 is a proven SERCA activator with the promising effect of increasing SERCA activity (*44*), which, in this study, was used to confirm that the SERCA pumps in that fiber were not damaged and also indicate the total activating potential of the SERCA.

Measurement of mitochondrial functions

Respiration and ROS production

Mitochondrial function was measured in permeabilized muscle fibers, similar to the protocol that has been previously described by our laboratory (*4*). Briefly, red GTN muscle was excised from the body, and a small piece of muscle was used and finely dissected to separate the muscle fibers along their striations in cold buffer X containing 7.23 mM K_2EGTA, 2.77 mM CaK_2EGTA, 20 mM imidazole, 0.5 mM DTT, 20 mM taurine, 5.7 mM ATP, 14.3 mM PCr, 6.56 mM $MgCl_2$-$6H_2O$, and 50 mM K-MES (pH 7.1). Saponin (30 μg/ml) was added to the fibers to induce permeabilization for 30 min, followed by three 5-min washes in washing buffer containing 105 mM K-MES, 30 mM KCl, 10 mM K_2HPO_4, 5 mM $MgCl_2$-$6H_2O$, bovine serum albumin (BSA; 0.5 mg/ml), and 0.1 mM EGTA (pH 7.1). After washing, the permeabilized fibers were placed into the Oxygraph-2k (O2K; Oroboros Instruments, Austria) following the

protocols described before (*57*). The OCR was determined using the oxygen probe, while the ROS production rate was measured by the O2k-Fluo LED2-Module Fluorescence-Sensor Green with Amplex UltraRed Reagent (Invitrogen, A36006). H_2O_2 standard was measured each time before the actual experiments to calibrate the level of H_2O_2. All data generated from O2k were normalized to the muscle wet weights and analyzed with the official O2k software, DatLab version 7.0.

Mitochondrial CRC

The calcium metabolism of mitochondria was detected through its CRC by challenging the mitochondria with a sequential addition of calcium chloride as we have previously described (*27*). The mitochondrial CRC was measured in isolated mitochondria from GTN muscle on the basis of an established method in our laboratory (*4*). Briefly, GTN muscle was dissected, weighed, and bathed in 150 mM KCl and placed in Chappell-Perry buffer containing 100 mM KCl, 50 mM tris, 5 mM $MgCl_2$, 1 mM EDTA, and 1 mM ATP (pH 7.2), along with the protease from bovine pancreas (7.5 U/ml). The muscle was then chopped and homogenized, and the homogenate was centrifuged for 10 min at 600*g*, followed by the supernatant being passed through cheesecloth and centrifuged at 14,000*g* for 10 min. The resultant pellet was washed once in modified Chappell-Perry buffer, containing 100 mM KCl, 50 mM tris, 1 mM $MgCl_2$, 0.2 mM EDTA, and 1 mM ATP with 0.5% BSA, and once in modified Chappell-Perry buffer without BSA. After the mitochondrial isolation, protein concentration was estimated using Bradford assay, and the isolated mitochondria were used immediately in the CRC test. First, Calcium Green-5N, a membrane-impermeable calcium dye, was added into O2k chambers with the final concentration at 1 μM in 2 ml of CRC buffer [250 mM sucrose, 10 mM tris, and 10 mM KH_2PO_4 (pH 7.4)] containing substrates of mitochondrial complexes glutamate/malate (0.25 mM) and succinate (0.5 M). Mitochondria (with an equal amount of 100-μg protein) were then injected into the chamber with CRC buffer. After 5 min of thermal equilibration, 2.5 μM calcium chloride was added every 1 min until mitochondrial calcium release caused by PTP opening. CRC was determined by the cumulative amount of calcium taken by the mitochondria. It has been established previously that this value represents a reliable index of the calcium threshold for PTP opening in the whole mitochondrial population studied (*58*) and that calcium release is accompanied by complete loss of membrane potential and high-amplitude swelling of the matrix (*59*), which are hallmarks of permeability transition.

Histological staining

Confocal microscopy for NMJ morphology

GTN muscle was excised from the body, and then, small muscle pieces were taken under the cold phosphate-buffered saline (PBS) in a petri dish along the fiber directions with a careful removal of fat and connective tissues. Muscle samples were then transferred into a 24-well plate with 10% STUmol (Poly Scientific R&D, #2832) for 1 hour to fix the tissue with gentle shaking. After the fixation, the tissues were washed three times for 5 min in PBS at room temperature, followed by the tissue permeabilization under the 2% Triton in PBS for 30 min on a shaker. After permeabilization, the tissues were placed into the blocking buffer containing 4% BSA, 1% Triton, and 5% serum, which matches the host of secondary antibody (in this study, it is goat) diluted in PBS, blocking overnight in the cold room at 4°C. After blocking, primary antibodies were added as follows: 1:50 SV2 [Developmental Studies Hybridoma Bank (DSHB)] for nerve terminals and 1:50 2H3 (DSHB) for neurofilaments. The tissues were incubated overnight at 4°C, washed six times for 30 min in PBS at room temperature, and subsequently incubated with the secondary antibodies BTX-Alexa Fluor 488 (1:100; Invitrogen, #B13422) and goat anti-mouse Cy3 (1:250). After the incubation for secondary antibodies overnight at 4°C, all tissues were then washed six times for 30 min with PBS. Afterward, tissues were transferred onto slides, mounted with mounting medium, and sealed with nail polish. NMJ images were taken using the Nikon confocal microscope (Nikon Eclipse) under ×20 magnification, and *Z*-stacks were taken to show the 3D structure of intact NMJ. The total thickness of optical sections is around 20 to 60 μm, and the stack interval was set at every 1 to 2 μm, so there are around 20 to 30 images per stack. When analyzing the image, the NMJ area was first analyzed with the area occupied by each individual labeled AChR, for only the forward-facing NMJs. Then, the fragmentation level was quantified by counting the fragmented pieces of each NMJ, and if there are five or more pieces per junction, then the NMJ is considered as a fragmented NMJ. The denervation score was quantified as follows: score 0, there is no denervation, and the NMJ is fully overlapped with neural filament; score 1, partial denervation and the NMJ is partially overlapped with neural filament; and score 2, complete denervation and the NMJ has no overlap with neural filament.

Fluorescent staining for calcium storage in muscle fiber bundles

Muscle fibers were dissected from the fast-twitch EDL muscle, and the fibers were bundled up with silk suture and permeabilized with the presence of saponin (30 μg/ml) in K-HDTA solution for 20 min and then incubated with Fluro-5F fluorescent dye (~5 μM, cell permeable; Invitrogen, Thermo Fisher Scientific, USA) for 10 min, followed by three 5-min washing steps. To detect the maximum calcium storage in SR, another set of permeabilized fiber bundles were first treated with loading solution to maximally load the SR with calcium for 180 s and then stained. Afterward, all fiber bundles were mounted onto slides, images were taken by the Nikon confocal microscope, and all images were taken at exactly the same condition to guarantee that the final calcium fluorescence is comparable. To include all calcium signals from the whole 3D structure of the fiber, *Z*-stacks were taken. The total thickness of fiber bundles is around 50 μm, and the stack interval was set at every 1 to 2 μm, so there are around 20 to 30 images per stack. Different calcium concentrations were analyzed by quantifying the total Ca^{2+} fluorescent intensity of each fiber bundle, and then, this intensity was normalized to the bundle size to give a specific Ca^{2+} fluorescence per fiber area. Through comparing this specific Ca^{2+} fluorescence, we were then able to detect the relative SR Ca^{2+} storage in different groups at both endogenous and maximum levels. The statistical analysis for all images taken in this section was done by ImageJ software (ImageJ).

Western blotting and antibody information

All samples used for Western blot analysis were performed with GTN muscle. Furthermore, samples were collected specifically from the mixed and white portions of the GTN [which represent predominantly type IIB fast-twitch fibers (*60*)], as we described previously (*15*). In general, GTN muscle tissues were homogenized in radioimmunoprecipitation assay buffer containing 50 mM tris (pH 7.4), 140 mM NaCl, 1 mM EDTA, 0.5 mM EGTA, 50 mM NaF, 1 mM NaO vanadate, 1% mM IGEPAL [octylphenoxy poly(ethyleneoxy)ethanol, branched],

and protease inhibitors. Total protein of homogenates was quantified with the Bradford protein assay kit (Sigma-Aldrich, Poole, UK), and the same amount of protein was loaded and separated with SDS–polyacrylamide gel electrophoresis (SDS-PAGE) gels at certain percentages, i.e., 10 or 12%. Instead of muscle homogenates, the determination of *S*-glutathionylation was performed using single skinned fiber bundles. Skinned fibers were bundled up with silk suture, and after the DTDP-GSH treatment, fiber bundles were processed with nonreducing buffer [containing 125 mM tris (pH 6.8), 10% glycerol, 4% SDS, 0.01% bromophenol blue, and 5 mM *N*-ethylmaleimide] for SDS-PAGE gels. All SDS-PAGE gels were run at 200 V for 1 hour and wet-transferred onto 0.45-μm nitrocellulose membranes (Bio-Rad) with the conditions of 100 V, 30 min at 4°C, same as described before (*22*). After the transfer, total proteins in each lane was quantified using Ponceau S staining (Sigma-Aldrich, #P3504); then, the Ponceau S on the membrane was removed with double distilled water washing, and the membrane was then blocked with 1% BSA solution in Tris buffered saline with Tween (TBST) for at least 1 hour at room temperature. After the blocking, primary antibodies were added onto the membrane and incubated overnight at 4°C. After the primary antibody incubation, the membrane was washed with blocking buffer and then exposed to the secondary antibody for another 30 to 60 min. After the secondary antibody, membrane was washed with TBST for the last time to clean the background. Protein bands were visualized and quantified using the GeneTools system (Syngene, Frederick, MD, USA). The relative content of each protein measured using Western blot analysis was normalized to sample total protein content measured using Ponceau S stain and densitometry of total Ponceau S in that sample lane. Primary antibody information was as follows: *Sod1* (Enzo, #ADI-SOD-101-E), SERCA1 (DSHB, #CAF2-5D2), SERCA2a (Cell Signaling Technology, #4388S), CSQ1/2 (Abcam, #ab3516), parvalbumin (Abcam, #ab11427), RyR (DSHB, #34C), DHPRα (DSHB, #IIID5E1), NKAα1 (Cell Signaling Technology, #3010), NKAα2 (Merck Millipore, #07-674), calstabin (FKBP12) (Abcam, #ab2918), GSH (ViroGen, #101-A), and TnI (Cell Signaling Technology, #4002).

Statistical analysis

All results are presented as mean values ± SD, and comparisons among different groups were performed with one-way analysis of variance (ANOVA) and Tukey's multiple comparisons test. The statistical analysis was undertaken using GraphPad Prism 8, and the statistical significance was set at P values less than 0.05.

SUPPLEMENTARY MATERIALS

Supplementary material for this article is available at https://science.org/doi/10.1126/sciadv.add7377

View/request a protocol for this paper from *Bio-protocol*.

REFERENCES AND NOTES

1. R. Qaisar, S. Bhaskaran, P. Premkumar, R. Ranjit, K. S. Natarajan, B. Ahn, K. Riddle, D. R. Claflin, A. Richardson, S. V. Brooks, H. van Remmen, Oxidative stress-induced dysregulation of excitation-contraction coupling contributes to muscle weakness. *J. Cachexia. Sarcopenia Muscle* **9**, 1003–1017 (2018).
2. W. K. Mitchell, J. Williams, P. Atherton, M. Larvin, J. Lund, M. Narici, Sarcopenia, dynapenia, and the impact of advancing age on human skeletal muscle size and strength; a quantitative review. *Front. Physiol.* **3**, 260 (2012).
3. Y. Zhang, C. Davis, G. K. Sakellariou, Y. Shi, A. C. Kayani, D. Pulliam, A. Bhattacharya, A. Richardson, M. J. Jackson, A. McArdle, S. V. Brooks, H. van Remmen, CuZnSOD gene deletion targeted to skeletal muscle leads to loss of contractile force but does not cause muscle atrophy in adult mice. *FASEB J.* **27**, 3536–3548 (2013).
4. B. Ahn, R. Ranjit, P. Premkumar, G. Pharaoh, K. M. Piekarz, S. Matsuzaki, D. R. Claflin, K. Riddle, J. Judge, S. Bhaskaran, K. S. Natarajan, E. Barboza, B. Wronowski, M. Kinter, K. M. Humphries, T. M. Griffin, W. M. Freeman, A. Richardson, S. V. Brooks, H. van Remmen, Mitochondrial oxidative stress impairs contractile function but paradoxically increases muscle mass via fibre branching. *J. Cachexia. Sarcopenia Muscle* **10**, 411–428 (2019).
5. G. K. Sakellariou, B. McDonagh, H. Porter, I. I. Giakoumaki, K. E. Earl, G. A. Nye, A. Vasilaki, S. V. Brooks, A. Richardson, H. van Remmen, A. McArdle, M. J. Jackson, Comparison of whole body SOD1 knockout with muscle-specific SOD1 knockout mice reveals a role for nerve redox signaling in regulation of degenerative pathways in skeletal muscle. *Antioxid. Redox Signal.* **28**, 275–295 (2018).
6. K. Sataranatarajan, R. Qaisar, C. Davis, G. K. Sakellariou, A. Vasilaki, Y. Zhang, Y. Liu, S. Bhaskaran, A. McArdle, M. Jackson, S. V. Brooks, A. Richardson, H. van Remmen, Neuron specific reduction in CuZnSOD is not sufficient to initiate a full sarcopenia phenotype. *Redox Biol.* **5**, 140–148 (2015).
7. G. K. Sakellariou, C. S. Davis, Y. Shi, M. V. Ivannikov, Y. Zhang, A. Vasilaki, G. T. Macleod, A. Richardson, H. van Remmen, M. J. Jackson, A. McArdle, S. V. Brooks, Neuron-specific expression of CuZnSOD prevents the loss of muscle mass and function that occurs in homozygous CuZnSOD-knockout mice. *FASEB J.* **28**, 1666–1681 (2014).
8. S. Bhaskaran, N. Pollock, P. C. Macpherson, B. Ahn, K. M. Piekarz, C. A. Staunton, J. L. Brown, R. Qaisar, A. Vasilaki, A. Richardson, A. M. Ardle, M. J. Jackson, S. V. Brooks, H. Van Remmen, Neuron-specific deletion of CuZnSOD leads to an advanced sarcopenic phenotype in older mice. *Aging Cell* **19**, e13225 (2020).
9. Y. C. Jang, M. S. Lustgarten, Y. Liu, F. L. Muller, A. Bhattacharya, H. Liang, A. B. Salmon, S. V. Brooks, L. Larkin, C. R. Hayworth, A. Richardson, H. van Remmen, Increased superoxide in vivo accelerates age-associated muscle atrophy through mitochondrial dysfunction and neuromuscular junction degeneration. *FASEB J.* **24**, 1376–1390 (2010).
10. F. L. Muller, W. Song, Y. Liu, A. Chaudhuri, S. Pieke-Dahl, R. Strong, T. T. Huang, C. J. Epstein, L. J. Roberts II, M. Csete, J. A. Faulkner, H. van Remmen, Absence of CuZn superoxide dismutase leads to elevated oxidative stress and acceleration of age-dependent skeletal muscle atrophy. *Free Radic. Biol. Med.* **40**, 1993–2004 (2006).
11. S. S. Deepa, H. van Remmen, S. V. Brooks, J. A. Faulkner, L. Larkin, A. McArdle, M. J. Jackson, A. Vasilaki, A. Richardson, Accelerated sarcopenia in Cu/Zn superoxide dismutase knockout mice. *Free Radic. Biol. Med.* **132**, 19–23 (2019).
12. F. L. Muller, W. Song, Y. C. Jang, Y. Liu, M. Sabia, A. Richardson, H. van Remmen, Denervation-induced skeletal muscle atrophy is associated with increased mitochondrial ROS production. *Am. J. Physiol. Regul. Integr. Comp. Physiol.* **293**, R1159–R1168 (2007).
13. G. Pharaoh, J. L. Brown, K. Sataranatarajan, P. Kneis, J. Bian, R. Ranjit, N. Hadad, C. Georgescu, P. Rabinovitch, Q. Ran, J. D. Wren, W. Freeman, M. Kinter, A. Richardson, H. Van Remmen, Targeting cPLA$_2$ derived lipid hydroperoxides as a potential intervention for sarcopenia. *Sci. Rep.* **10**, 13968 (2020).
14. G. D. Lamb, Excitation-contraction coupling and fatigue mechanisms in skeletal muscle: Studies with mechanically skinned fibres. *J. Muscle Res. Cell Motil.* **23**, 81–91 (2002).
15. H. Xu, R. Ranjit, A. Richardson, H. Van Remmen, Muscle mitochondrial catalase expression prevents neuromuscular junction disruption, atrophy, and weakness in a mouse model of accelerated sarcopenia. *J. Cachexia. Sarcopenia Muscle* **12**, 1582–1596 (2021).
16. R. Qaisar, S. Bhaskaran, R. Ranjit, K. Sataranatarajan, P. Premkumar, K. Huseman, H. van Remmen, Restoration of SERCA ATPase prevents oxidative stress-related muscle atrophy and weakness. *Redox Biol.* **20**, 68–74 (2019).
17. L. M. Larkin, C. S. Davis, C. Sims-Robinson, T. Y. Kostrominova, H. Van Remmen, A. Richardson, E. L. Feldman, S. V. Brooks, Skeletal muscle weakness due to deficiency of CuZn-superoxide dismutase is associated with loss of functional innervation. *Am. J. Physiol. Reg. Integr. Comp. Physiol.* **301**, R1400–R1407 (2011).
18. M. J. Jackson, A. McArdle, Role of reactive oxygen species in age-related neuromuscular deficits. *J. Physiol.* **594**, 1979–1988 (2016).
19. J. P. Mollica, T. L. Dutka, T. L. Merry, C. R. Lamboley, G. K. McConell, M. J. McKenna, R. M. Murphy, G. D. Lamb, S-glutathionylation of troponin I (fast) increases contractile apparatus $Ca2^+$ sensitivity in fast-twitch muscle fibres of rats and humans. *J. Physiol.* **590**, 1443–1463 (2012).
20. C. R. Lamboley, V. L. Wyckelsma, T. L. Dutka, M. J. McKenna, R. M. Murphy, G. D. Lamb, Contractile properties and sarcoplasmic reticulum calcium content in type I and type II skeletal muscle fibres in active aged humans. *J. Physiol.* **593**, 2499–2514 (2015).
21. H. Xu, G. D. Lamb, R. M. Murphy, Changes in contractile and metabolic parameters of skeletal muscle as rats age from 3 to 12 months. *J. Muscle Res. Cell Motil.* **38**, 405–420 (2017).
22. H. Xu, X. Ren, G. D. Lamb, R. M. Murphy, Physiological and biochemical characteristics of skeletal muscles in sedentary and active rats. *J. Muscle Res. Cell Motil.* **39**, 1–16 (2018).
23. T. Adachi, R. M. Weisbrod, D. R. Pimentel, J. Ying, V. S. Sharov, C. Schöneich, R. A. Cohen, S-Glutathiolation by peroxynitrite activates SERCA during arterial relaxation by nitric oxide. *Nat. Med.* **10**, 1200–1207 (2004).
24. E. S. Dremina, V. S. Sharov, M. J. Davies, C. Schoneich, Oxidation and inactivation of SERCA by selective reaction of cysteine residues with amino acid peroxides. *Chem. Res. Toxicol.* **20**, 1462–1469 (2007).

25. F. Qin, D. A. Siwik, S. Lancel, J. Zhang, G. M. Kuster, I. Luptak, L. Wang, X. Tong, Y. J. Kang, R. A. Cohen, W. S. Colucci, Hydrogen peroxide-mediated SERCA cysteine 674 oxidation contributes to impaired cardiac myocyte relaxation in senescent mouse heart. *J. Am. Heart Assoc.* **2**, e000184 (2013).
26. V. S. Sharov, E. S. Dremina, N. A. Galeva, T. D. Williams, C. Schöneich, Quantitative mapping of oxidation-sensitive cysteine residues in SERCA in vivo and in vitro by HPLC-electrospray-tandem MS: Selective protein oxidation during biological aging. *Biochem. J.* **394**, 605–615 (2006).
27. B. Ahn, R. Ranjit, P. Kneis, H. Xu, K. M. Piekarz, W. M. Freeman, M. Kinter, A. Richardson, Q. Ran, S. V. Brooks, H. Van Remmen, Scavenging mitochondrial hydrogen peroxide by peroxiredoxin 3 overexpression attenuates contractile dysfunction and muscle atrophy in a murine model of accelerated sarcopenia. *Aging Cell* **21**, e13569 (2022).
28. Y. C. Jang, Y. Liu, C. R. Hayworth, A. Bhattacharya, M. S. Lustgarten, F. L. Muller, A. Chaudhuri, W. Qi, Y. Li, J. Y. Huang, E. Verdin, A. Richardson, H. van Remmen, Dietary restriction attenuates age-associated muscle atrophy by lowering oxidative stress in mice even in complete absence of CuZnSOD. *Aging Cell* **11**, 770–782 (2012).
29. D. A. Lowe, A. D. Husom, D. A. Ferrington, L. V. Thompson, Myofibrillar myosin ATPase activity in hindlimb muscles from young and aged rats. *Mech. Ageing Dev.* **125**, 619–627 (2004).
30. G. D. Lamb, D. G. Stephenson, Measurement of force and calcium release using mechanically skinned fibers from mammalian skeletal muscle. *J. Appl. Physiol.* **125**, 1105–1127 (2018).
31. G. S. Posterino, G. D. Lamb, Effect of sarcoplasmic reticulum $Ca2^+$ content on action potential-induced $Ca2^+$ release in rat skeletal muscle fibres. *J. Physiol.* **551**, 219–237 (2003).
32. K. Araki, H. Kusano, N. Sasaki, R. Tanaka, T. Hatta, K. Fukui, T. Natsume, Redox sensitivities of global cellular cysteine residues under reductive and oxidative stress. *J. Proteome Res.* **15**, 2548–2559 (2016).
33. P. A. Kramer, J. Duan, M. J. Gaffrey, A. K. Shukla, L. Wang, T. K. Bammler, W. J. Qian, D. J. Marcinek, Fatiguing contractions increase protein S-glutathionylation occupancy in mouse skeletal muscle. *Redox Biol.* **17**, 367–376 (2018).
34. R. M. Murphy, T. L. Dutka, G. D. Lamb, Hydroxyl radical and glutathione interactions alter calcium sensitivity and maximum force of the contractile apparatus in rat skeletal muscle fibres. *J. Physiol.* **586**, 2203–2216 (2008).
35. E. Verburg, R. M. Murphy, I. Richard, G. D. Lamb, Involvement of calpains in $Ca2^+$-induced disruption of excitation-contraction coupling in mammalian skeletal muscle fibers. *Am. J. Physiol. Cell Physiol.* **296**, C1115–C1122 (2009).
36. R. M. Murphy, E. Verburg, G. D. Lamb, $Ca2^+$ activation of diffusible and bound pools of mu-calpain in rat skeletal muscle. *J. Physiol.* **576**, 595–612 (2006).
37. T. H. Pedersen, O. B. Nielsen, G. D. Lamb, D. G. Stephenson, Intracellular acidosis enhances the excitability of working muscle. *Science* **305**, 1144–1147 (2004).
38. B. D. Perry, V. L. Wyckelsma, R. M. Murphy, C. H. Steward, M. Anderson, I. Levinger, A. C. Petersen, M. J. McKenna, Dissociation between short-term unloading and resistance training effects on skeletal muscle Na^+, K^+-ATPase, muscle function, and fatigue in humans. *J. Appl. Physiol.* **121**, 1074–1086 (2016).
39. V. L. Wyckelsma, B. D. Perry, J. Bangsbo, M. J. McKenna, Inactivity and exercise training differentially regulate abundance of Na^+-K^+-ATPase in human skeletal muscle. *J. Appl. Physiol. (1985)* **127**, 905–920 (2019).
40. D. E. Bartlett, R. B. Miller, S. Thiesfeldt, H. V. Lakhani, J. I. Shapiro, K. Sodhi, The role of Na/K-ATPase signaling in oxidative stress related to aging: Implications in obesity and cardiovascular disease. *Int. J. Mol. Sci.* **19**, 2139 (2018).
41. Y. Yan, J. I. Shapiro, The physiological and clinical importance of sodium potassium ATPase in cardiovascular diseases. *Curr. Opin. Pharmacol.* **27**, 43–49 (2016).
42. K. Sodhi, A. Nichols, A. Mallick, R. L. Klug, J. Liu, X. Wang, K. Srikanthan, P. Goguet-Rubio, A. Nawab, R. Pratt, M. N. Lilly, J. R. Sanabria, Z. Xie, N. G. Abraham, J. I. Shapiro, The Na/K-ATPase oxidant amplification loop regulates aging. *Sci. Rep.* **8**, 9721 (2018).
43. S. Gehlert, W. Bloch, F. Suhr, $Ca2^+$-dependent regulations and signaling in skeletal muscle: From electro-mechanical coupling to adaptation. *Int. J. Mol. Sci.* **16**, 1066–1095 (2015).
44. R. Qaisar, G. Pharaoh, S. Bhaskaran, H. Xu, R. Ranjit, J. Bian, B. Ahn, C. Georgescu, J. D. Wren, H. Van Remmen, Restoration of sarcoplasmic reticulum $Ca2^+$ ATPase (SERCA) activity prevents age-related muscle atrophy and weakness in mice. *Int. J. Mol. Sci.* **22**, 37 (2021).
45. R. Qaisar, M. Qayum, T. Muhammad, Reduced sarcoplasmic reticulum $Ca2^+$ ATPase activity underlies skeletal muscle wasting in asthma. *Life Sci.* **273**, 119296 (2021).
46. H. Xu, H. Van Remmen, The SarcoEndoplasmic reticulum calcium ATPase (SERCA) pump: A potential target for intervention in aging and skeletal muscle pathologies. *Skelet. Muscle* **11**, 25 (2021).
47. E. A. Permyakov, V. N. Uversky, S. E. Permyakov, Parvalbumin as a pleomorphic protein. *Curr. Protein Pept. Sci.* **18**, 780–794 (2017).
48. S. Boncompagni, F. Protasi, C. Franzini-Armstrong, Sequential stages in the age-dependent gradual formation and accumulation of tubular aggregates in fast twitch muscle fibers: SERCA and calsequestrin involvement. *Age (Dordr.)* **34**, 27–41 (2012).
49. O. Delbono, K. S. O'Rourke, W. H. Ettinger, Excitation-calcium release uncoupling in aged single human skeletal muscle fibers. *J. Membr. Biol.* **148**, 211–222 (1995).
50. D. C. Andersson, M. J. Betzenhauser, S. Reiken, A. C. Meli, A. Umanskaya, W. Xie, T. Shiomi, R. Zalk, A. Lacampagne, A. R. Marks, Ryanodine receptor oxidation causes intracellular calcium leak and muscle weakness in aging. *Cell Metab.* **14**, 196–207 (2011).
51. R. Bravo-Sagua, V. Parra, C. López-Crisosto, P. Díaz, A. F. Quest, S. Lavandero, Calcium transport and signaling in mitochondria. *Compr. Physiol.* **7**, 623–634 (2017).
52. M. Picard, D. Ritchie, M. M. Thomas, K. J. Wright, R. T. Hepple, Alterations in intrinsic mitochondrial function with aging are fiber type-specific and do not explain differential atrophy between muscles. *Aging Cell* **10**, 1047–1055 (2011).
53. S. Elchuri, T. D. Oberley, W. Qi, R. S. Eisenstein, L. J. Roberts, H. van Remmen, C. J. Epstein, T. T. Huang, CuZnSOD deficiency leads to persistent and widespread oxidative damage and hepatocarcinogenesis later in life. *Oncogene* **24**, 367–380 (2005).
54. D. G. Stephenson, D. A. Williams, Calcium-activated force responses in fast- and slow-twitch skinned muscle fibres of the rat at different temperatures. *J. Physiol.* **317**, 281–302 (1981).
55. R. M. Murphy, N. T. Larkins, J. P. Mollica, N. A. Beard, G. D. Lamb, Calsequestrin content and SERCA determine normal and maximal $Ca2^+$ storage levels in sarcoplasmic reticulum of fast- and slow-twitch fibres of rat. *J. Physiol.* **587**, 443–460 (2009).
56. M. Chua, A. F. Dulhunty, Inactivation of excitation-contraction coupling in rat extensor digitorum longus and soleus muscles. *J. Gen. Physiol.* **91**, 737–757 (1988).
57. G. Krumschnabel, M. Fontana-Ayoub, Z. Sumbalova, J. Heidler, K. Gauper, M. Fasching, E. Gnaiger, Simultaneous high-resolution measurement of mitochondrial respiration and hydrogen peroxide production. *Methods Mol. Biol.* **1264**, 245–261 (2015).
58. K. Csukly, A. Ascah, J. Matas, P. F. Gardiner, E. Fontaine, Y. Burelle, Muscle denervation promotes opening of the permeability transition pore and increases the expression of cyclophilin D. *J. Physiol.* **574**, 319–327 (2006).
59. M. Marcil, K. Bourduas, A. Ascah, Y. Burelle, Exercise training induces respiratory substrate-specific decrease in $Ca2^+$-induced permeability transition pore opening in heart mitochondria. *Am. J. Physiol. Heart Circ. Physiol.* **290**, H1549–H1557 (2006).
60. D. Bloemberg, J. Quadrilatero, Rapid determination of myosin heavy chain expression in rat, mouse, and human skeletal muscle using multicolor immunofluorescence analysis. *PLOS ONE* **7**, e35273 (2012).

Acknowledgments

Funding: This work was supported by a P01 grant (NIA-AG051442) and R01 grant (NIA-AG050676) from NIA, VA merit grant (I01BX004453), and the VA Senior Career Scientist award (IK6 BX005234) to H.V.R. **Author contributions:** H.X., B.A., and H.V.R. contributed in the conception and design of the research. H.X. and B.A. performed the experiments and analyzed the data. H.X., B.A., and H.V.R. interpreted the results of the experiments. H.X., B.A., and H.V.R. prepared the figures and drafted the manuscript. H.X., B.A., and H.V.R edited and revised the manuscript, and all authors approved the final version of the manuscript. **Competing interests:** The authors declare that they have no competing interests. **Data and materials availability:** All data needed to evaluate the conclusions in the paper are present in the paper and/or the Supplementary Materials.

Submitted 30 June 2022
Accepted 8 September 2022
Published 26 October 2022
10.1126/sciadv.add7377